



Pedro Lima Vaz Jannuzzi

**Study of Numerical Methods for Modeling
Electromagnetic Wave Propagation in Curved
Waveguides with Rectangular Cross-Section**

Dissertação de Mestrado

Thesis presented to the Programa de Pós-graduação em Engenharia de Elétrica, do Departamento de Engenharia Elétrica da PUC-Rio in partial fulfillment of the requirements for the degree of Mestre em Engenharia de Elétrica.

Advisor : Prof. José Ricardo Bergmann
Co-advisor: Prof. Guilherme Simon da Rosa

Rio de Janeiro
February 2025



Pedro Lima Vaz Jannuzzi

**Study of Numerical Methods for Modeling
Electromagnetic Wave Propagation in Curved
Waveguides with Rectangular Cross-Section**

Thesis presented to the Programa de Pós-graduação em Engenharia de Elétrica da PUC-Rio in partial fulfillment of the requirements for the degree of Mestre em Engenharia de Elétrica. Approved by the Examination Committee:

Prof. José Ricardo Bergmann

Advisor

Departamento de Engenharia Elétrica – PUC-Rio

Prof. Guilherme Simon da Rosa

Dep. de Eng. Eletrônica e de Telecomunicações – UNESP

Prof. Rafael Abrantes Penchel

Dep. de Eng. Eletrônica e de Telecomunicações – UNESP

Prof. Raul Oliveira Ribeiro

Dep. de Eng. Eletrônica e de Telecomunicações – UNESP

Rio de Janeiro, February the 4th, 2025

All rights reserved.

Pedro Lima Vaz Jannuzzi

Received the B.S. degree in electrical engineering from the Pontifical Catholic University of Rio de Janeiro, Rio de Janeiro, Brazil, in 2023.

Bibliographic data

Lima Vaz Jannuzzi, Pedro

Study of Numerical Methods for Modeling Electromagnetic Wave Propagation in Curved Waveguides with Rectangular Cross-Section / Pedro Lima Vaz Jannuzzi; advisor: José Ricardo Bergmann; co-advisor: Guilherme Simon da Rosa. – 2025.

49 f: il. color. ; 30 cm

Dissertação (mestrado) - Pontifícia Universidade Católica do Rio de Janeiro, Departamento de Engenharia Elétrica, 2025.

Inclui bibliografia

1. Engenharia Elétrica – Teses. 2. Guias de onda retangulares curvados. 3. Método de Point Matching. 4. Método dos Momentos. 5. Sistema de coordenadas curvado. 6. Raio de curvatura.
I. Bergmann, José Ricardo. II. Rosa, Guilherme Simon da. III. Pontifícia Universidade Católica do Rio de Janeiro. Departamento de Engenharia Elétrica. IV. Título.

CDD: 621.3

To my parents, for their
unconditional support.

Acknowledgments

First, I would like to express my sincere gratitude to my advisor, José Ricardo Bergmann, and co-advisor, Guilherme Simon da Rosa, for the guidance, support, encouragement, and motivation they provided me throughout these research semesters, which will undoubtedly benefit me in various aspects of my future academic career.

I am also thankful to the members of my examining committee for their thorough evaluation and constructive feedback.

I am grateful to all the professors in the Department of Electrical Engineering at PUC-Rio for their teachings and friendship.

My deep gratitude to my family and friends for their support during this journey.

Lastly, I would like to extend a special thank you to PUC-Rio for the waiver of school fees provided by the Graduate Program in Electrical Engineering and for all the infrastructure offered for the completion of this thesis.

This study was financed in part by the Coordenação de Aperfeiçoamento de Pessoal de Nível Superior - Brasil (CAPES) - Finance Code 001.

Abstract

Lima Vaz Jannuzzi, Pedro; Bergmann, José Ricardo (Advisor); Rosa, Guilherme Simon da (Co-Advisor). **Study of Numerical Methods for Modeling Electromagnetic Wave Propagation in Curved Waveguides with Rectangular Cross-Section**. Rio de Janeiro, 2025. 49p. Dissertação de Mestrado – Departamento de Engenharia Elétrica, Pontifícia Universidade Católica do Rio de Janeiro.

This research presents case studies of engineering applications, such as electromagnetic propagation in uniformly curved waveguides with rectangular cross-sections, operating at typical frequencies of 5G and 6G mobile network systems. In this work, we introduce the boundary value problem and address numerical techniques for solving the Maxwell's equations in curved waveguides, aiming for solutions to the associated eigenvalue problem. First, the Point Matching method is employed as an alternative to solve this type of problem by tracking zeros of the determinant of a matrix. Next, we use the Method of Moments to solve the same problem by computing surface integrals of functions over the rectangular geometry. Additionally, this method is employed because it deals with a linear eigenvalue problem, making it more practical than Point Matching. Finally, using a computational algorithm developed in Matlab, we present a series of results on the electromagnetic propagation of the curved rectangular waveguide in the H-plane and E-plane for different values of the curvature radius of the curved rectangular section. The numerical results demonstrate the convergence of the presented solution with respect to the exact solution using a small number of harmonics.

Keywords

Curved Rectangular Waveguides; Point Matching Method; Method of Moments; Curved coordinate system; Radius of curvature; Electromagnetic propagation.

Resumo

Lima Vaz Jannuzzi, Pedro; Bergmann, José Ricardo; Rosa, Guilherme Simon da. **Estudo de métodos numéricos para a modelagem da propagação eletromagnética em guias de ondas curvados de seção transversal retangular**. Rio de Janeiro, 2025. 49p. Dissertação de Mestrado – Departamento de Engenharia Elétrica, Pontifícia Universidade Católica do Rio de Janeiro.

Esta pesquisa apresenta casos de estudo de aplicações de engenharia, como a propagação eletromagnética em guias de onda uniformemente curvados com seção transversal retangular, operando em frequências típicas dos sistemas de rede móvel 5G e 6G. Neste trabalho, apresentamos o problema de valor de contorno e abordamos técnicas numéricas para resolver as equações de Maxwell em guias de onda curvados, visando soluções para o problema de autovalores associado. Primeiro, o método de Point Matching é empregado como uma alternativa para resolver esse tipo de problema por meio do rastreamento de zeros do determinante de uma matriz. Em seguida, utilizamos o Método dos Momentos para resolver esse mesmo problema, por meio do cálculo de integrais de superfície das funções sobre a geometria retangular. Além disso, este método é utilizado por ser tratar de um problema de autovalor linear, tornando-o mais prático que o Point Matching. Por fim, mediante um algoritmo computacional desenvolvido em Matlab, apresentamos uma série de resultados da propagação eletromagnética do guia retangular curvado no plano H e no plano E para diferentes valores do raio de curvatura da seção retangular curvada. Os resultados numéricos evidenciam a convergência da solução apresentada em relação à solução exata com pequena quantidade de harmônicos.

Palavras-chave

Guias de onda retangulares curvados; Método de Point Matching; Método dos Momentos; Sistema de coordenadas curvado; Raio de curvatura.

Table of contents

| | | |
|----------|---|-----------|
| 1 | Introduction | 12 |
| 1.1 | General Introduction | 12 |
| 1.2 | Thesis Organization | 13 |
| 2 | Point Matching Method | 15 |
| 2.1 | Solution through Decomposition of the y Component | 15 |
| 2.2 | Numerical Results | 18 |
| 2.2.1 | H-Plane with $R = 2a$ | 18 |
| 2.2.2 | E-Plane with $R = 2a$ | 20 |
| 2.2.3 | H-Plane with $R = a$ | 20 |
| 2.2.4 | E-Plane with $R = a$ | 20 |
| 2.2.5 | H-Plane with $R = 0.75a$ | 21 |
| 2.2.6 | E-Plane with $R = 0.75a$ | 22 |
| 2.2.7 | H-Plane with $R = 10a$ | 22 |
| 2.2.8 | E-Plane with $R = 10a$ | 23 |
| 3 | Method of Moments | 27 |
| 3.1 | Solution of the Linear Eigenvalue Problem | 28 |
| 3.2 | Numerical Results | 30 |
| 3.2.1 | H-Plane with $R = 2a$ | 30 |
| 3.2.2 | E-Plane with $R = 2a$ | 31 |
| 3.2.3 | H-Plane with $R = a$ | 32 |
| 3.2.4 | E-Plane with $R = a$ | 33 |
| 3.2.5 | H-Plane with $R = 0.75a$ | 34 |
| 3.2.6 | E-Plane with $R = 0.75a$ | 36 |
| 3.2.7 | H-Plane with $R = 10a$ | 37 |
| 3.2.8 | E-Plane with $R = 10a$ | 38 |
| 4 | Comparison between the two methods presented | 41 |
| 4.1 | Relative Error | 41 |
| 4.2 | Simulation Time | 41 |
| 5 | Conclusions | 45 |
| | Bibliography | 46 |

List of figures

| | | |
|------------|--|----|
| Figure 2.1 | Geometry of a rectangular waveguide curved in the (a) E-plane and (b) H-plane. | 15 |
| Figure 2.2 | Normalized fields $ e_y(x) $ for the $\text{TM}_{1,0}^y$, $\text{TM}_{2,0}^y$ and $\text{TM}_{3,0}^y$ modes, for $a > b$, $R = 2a$ and $P = 20$ points. | 19 |
| Figure 2.3 | Normalized fields $ h_y(x) $ for the $\text{TE}_{0,1}^y$, $\text{TE}_{1,1}^y$ and $\text{TE}_{2,1}^y$ modes, for $a < b$, $R = 2a$ and $P = 20$ points. | 20 |
| Figure 2.4 | Normalized fields $ e_y(x) $ for the $\text{TM}_{1,0}^y$, $\text{TM}_{2,0}^y$ and $\text{TM}_{3,0}^y$ modes, for $a > b$, $R = a$ and $P = 20$ points. | 21 |
| Figure 2.5 | Normalized fields $ h_y(x) $ for the $\text{TE}_{0,1}^y$, $\text{TE}_{1,1}^y$, and $\text{TE}_{2,1}^y$ modes, for $a < b$, $R = a$ and $P = 20$ points. | 22 |
| Figure 2.6 | Normalized fields $ e_y(x) $ for the $\text{TM}_{1,0}^y$, $\text{TM}_{2,0}^y$ and $\text{TM}_{3,0}^y$ modes, for $a > b$, $R = 0.75a$ and $P = 20$ points. | 23 |
| Figure 2.7 | Normalized fields $ h_y(x) $ for the $\text{TE}_{0,1}^y$, $\text{TE}_{1,1}^y$ and $\text{TE}_{2,1}^y$ modes, for $a < b$, $R = 0.75a$ and $P = 20$ points. | 24 |
| Figure 2.8 | Normalized fields $ e_y(x) $ for the $\text{TM}_{1,0}^y$, $\text{TM}_{2,0}^y$ and $\text{TM}_{3,0}^y$ modes, for $a > b$, $R = 10a$ and $P = 20$ points. | 24 |
| Figure 2.9 | Normalized fields $ h_y(x) $ for the $\text{TE}_{0,1}^y$, $\text{TE}_{1,1}^y$ and $\text{TE}_{2,1}^y$ modes, for $a < b$, $R = 10a$ and $P = 20$ points. | 24 |
| Figure 3.1 | Relative error (%) of the normalized field curves $ e_y(x) $ between PMM and MoM for $\text{TM}_{1,0}^y$, $\text{TM}_{2,0}^y$ and $\text{TM}_{3,0}^y$ modes, for $a > b$, $R = 2a$ and $P = 20$ points. | 31 |
| Figure 3.2 | Relative error (%) of the normalized field curves $ h_y(x) $ between PMM and MoM for $\text{TE}_{0,1}^y$, $\text{TE}_{1,1}^y$ and $\text{TE}_{2,1}^y$ modes, for $a > b$, $R = 2a$ and $P = 20$ points. | 33 |
| Figure 3.3 | Relative error (%) of the normalized field curves $ e_y(x) $ between PMM and MoM for $\text{TM}_{1,0}^y$, $\text{TM}_{2,0}^y$ and $\text{TM}_{3,0}^y$ modes, for $a > b$, $R = a$ and $P = 20$ points. | 34 |
| Figure 3.4 | Relative error (%) of the normalized field curves $ h_y(x) $ between PMM and MoM for $\text{TE}_{0,1}^y$, $\text{TE}_{1,1}^y$ and $\text{TE}_{2,1}^y$ modes, for $a > b$, $R = a$ and $P = 20$ points. | 35 |
| Figure 3.5 | Relative error (%) of the normalized field curves $ e_y(x) $ between PMM and MoM for $\text{TM}_{1,0}^y$, $\text{TM}_{2,0}^y$ and $\text{TM}_{3,0}^y$ modes, for $a > b$, $R = 0.75a$ and $P = 20$ points. | 36 |
| Figure 3.6 | Relative error (%) of the normalized field curves $ h_y(x) $ between PMM and MoM for $\text{TE}_{0,1}^y$, $\text{TE}_{1,1}^y$ and $\text{TE}_{2,1}^y$ modes, for $a > b$, $R = 0.75a$ and $P = 20$ points. | 38 |
| Figure 3.7 | Relative error (%) of the normalized field curves $ e_y(x) $ between PMM and MoM for $\text{TM}_{1,0}^y$, $\text{TM}_{2,0}^y$ and $\text{TM}_{3,0}^y$ modes, for $a > b$, $R = 10a$ and $P = 20$ points. | 39 |
| Figure 3.8 | Relative error (%) of the normalized field curves $ h_y(x) $ between PMM and MoM for $\text{TE}_{0,1}^y$, $\text{TE}_{1,1}^y$ and $\text{TE}_{2,1}^y$ modes, for $a > b$, $R = 10a$ and $P = 20$ points. | 40 |

List of tables

| | | |
|-----------|---|----|
| Table 2.1 | Normalized longitudinal wavenumbers k_ϕ/k and k_ζ/k for TM modes in a rectangular waveguide curved in the H-plane (with $R = 2a$) obtained respectively by the exact solution (using Bessel functions) in [11] and by our point matching method. | 19 |
| Table 2.2 | Normalized longitudinal wavenumbers k_ϕ/k and k_ζ/k for TE modes in a rectangular waveguide curved in the E-plane (with $R = 2a$) obtained respectively by the exact solution (using Bessel functions) in [11] and by our point matching method. | 21 |
| Table 2.3 | Normalized longitudinal wavenumbers k_ϕ/k and k_ζ/k for TM modes in a rectangular waveguide curved in the H-plane (with $R = a$) obtained respectively by the exact solution (using Bessel functions) in [11] and by our point matching method. | 22 |
| Table 2.4 | Normalized longitudinal wavenumbers k_ϕ/k and k_ζ/k for TE modes in a rectangular waveguide curved in the E-plane (with $R = a$) obtained respectively by the exact solution (using Bessel functions) in [11] and by our point matching method. | 23 |
| Table 2.5 | Normalized longitudinal wavenumbers k_ϕ/k and k_ζ/k for TM modes in a rectangular waveguide curved in the H-plane (with $R = 0.75a$) obtained respectively by the exact solution (using Bessel functions) in [11] and by our point matching method. | 25 |
| Table 2.6 | Normalized longitudinal wavenumbers k_ϕ/k and k_ζ/k for TE modes in a rectangular waveguide curved in the E-plane (with $R = 0.75a$) obtained respectively by the exact solution (using Bessel functions) in [11] and by our point matching method. | 25 |
| Table 2.7 | Normalized longitudinal wavenumbers k_ϕ/k and k_ζ/k for TM modes in a rectangular waveguide curved in the H-plane (with $R = 10a$) obtained respectively by the exact solution (using Bessel functions) in [11] and by our point matching method. | 26 |
| Table 2.8 | Normalized longitudinal wavenumbers k_ϕ/k and k_ζ/k for TE modes in a rectangular waveguide curved in the E-plane (with $R = 10a$) obtained respectively by the exact solution (using Bessel functions) in [11] and by our point matching method. | 26 |
| Table 3.1 | Normalized longitudinal wavenumbers k_ϕ/k and k_ζ/k for TM modes in a rectangular waveguide curved in the H-plane (with $R = 2a$) obtained respectively by the exact solution (using Bessel functions) in [11] and by the method of moments. | 30 |
| Table 3.2 | Normalized longitudinal wavenumbers k_ϕ/k and k_ζ/k for TE modes in a rectangular waveguide curved in the E-plane (with $R = 2a$) obtained respectively by the exact solution (using Bessel functions) in [11] and by the method of moments. | 32 |
| Table 3.3 | Normalized longitudinal wavenumbers k_ϕ/k and k_ζ/k for TM modes in a rectangular waveguide curved in the H-plane (with $R = a$) obtained respectively by the exact solution (using Bessel functions) in [11] and by the method of moments. | 32 |

| | | |
|------------|---|----|
| Table 3.4 | Normalized longitudinal wavenumbers k_ϕ/k and k_ζ/k for TE modes in a rectangular waveguide curved in the E-plane (with $R = a$) obtained respectively by the exact solution (using Bessel functions) in [11] and by the method of moments. | 34 |
| Table 3.5 | Normalized longitudinal wavenumbers k_ϕ/k and k_ζ/k for TM modes in a rectangular waveguide curved in the H-plane (with $R = 0.75a$) obtained respectively by the exact solution (using Bessel functions) in [11] and by the method of moments. | 35 |
| Table 3.6 | Normalized longitudinal wavenumbers k_ϕ/k and k_ζ/k for TE modes in a rectangular waveguide curved in the E-plane (with $R = 0.75a$) obtained respectively by the exact solution (using Bessel functions) in [11] and by the method of moments. | 37 |
| Table 3.7 | Normalized longitudinal wavenumbers k_ϕ/k and k_ζ/k for TM modes in a rectangular waveguide curved in the H-plane (with $R = 10a$) obtained respectively by the exact solution (using Bessel functions) in [11] and by the method of moments. | 37 |
| Table 3.8 | Normalized longitudinal wavenumbers k_ϕ/k and k_ζ/k for TE modes in a rectangular waveguide curved in the E-plane (with $R = 10a$) obtained respectively by the exact solution (using Bessel functions) in [11] and by the method of moments. | 39 |
| Table 4.1 | Relative errors of the PMM and MoM for the E-plane and $R = 0.75a$ | 41 |
| Table 4.2 | Relative errors of the PMM and MoM for the E-plane and $R = a$ | 42 |
| Table 4.3 | Relative errors of the PMM and MoM for the E-plane and $R = 2a$ | 42 |
| Table 4.4 | Relative errors of the PMM and MoM for the E-plane and $R = 10a$ | 42 |
| Table 4.5 | Relative errors of the PMM and MoM for the H-plane and $R = 0.75a$ | 43 |
| Table 4.6 | Relative errors of the PMM and MoM for the H-plane and $R = a$ | 43 |
| Table 4.7 | Relative errors of the PMM and MoM for the H-plane and $R = 2a$ | 43 |
| Table 4.8 | Relative errors of the PMM and MoM for the H-plane and $R = 10a$ | 44 |
| Table 4.9 | Comparison of simulation times between the PMM and MoM methods in the E-plane | 44 |
| Table 4.10 | Comparison of simulation times between the PMM and MoM methods in the H-plane | 44 |

1 Introduction

1.1 General Introduction

The study of electromagnetic propagation in guided media is a topic of interest for engineering due to its applications for the analysis and design of microwave devices for onboard, satellite, and ground-based applications. In addition to the analysis of waveguides with straight longitudinal axis, immediate demands for miniaturization make the use of curved devices increasingly necessary for modeling coupled microwave filters for applications in complex communication systems.

Through additive manufacturing technology, which allows for engineering modifications in device design and fabrication, it is possible to produce antennas and microwave devices with complex structures. This technology enables the creation of precise complex structures, facilitating the optimization of miniaturized designs for satellite communications operating in the Ka, Q, and V bands [1], and enabling the mass production of IoT (Internet of Things) devices for terrestrial applications. Therefore, this topic is of great technological importance for modeling devices for operation at millimeter-wave frequencies (30 GHz to 300 GHz), typical of 5G and 6G systems, as well as for research and development of low computational cost semi-analytical methods for electromagnetic propagation analysis.

In [2], equations for a rectangular waveguide with a straight longitudinal axis are analyzed, and in [3], the approach of precise numerical calculations was used on curves of rectangular-section waveguides. Lewin [4] derives approximate modal solutions for curves of the H and E planes through a perturbation analysis. In [5], a perturbation solution was obtained using a similar method. Weisshaar [6] presented a precise method based on the Mode Matching technique where the Helmholtz equation in the curved region is transformed into an eigenvalue problem.

Differently the conventional methodology, which employs the decomposition of fields in terms of decoupled TM and TE contributions, curved waveguides require the use of hybrid fields. A numerically stable formulation for

the analysis of electromagnetic fields in rectangular-section waveguides with a curved longitudinal axis is examined in [7–10]. In [11], this analysis is performed using Bessel functions to demonstrate that the formulation allows for more accurate representation of fields in uniformly curved rectangular waveguides compared to perturbation solutions.

The Method of Moments (MoM) and the Point Matching Method (PMM) are used in numerous works to model electromagnetic propagation in curved waveguides. In [12–14], PMM was employed to enforce boundary conditions at an appropriate set of points along the domain boundaries. This method applies when the contour of the waveguide’s cross-section is a closed curve, as seen in [15]. Ranade and Rosenfeld [16] proposed a point matching algorithm with consideration for the relative distance between points. In [6], a technique combining Mode Matching and MoM was used for the study of parallel curved waveguides.

The authors of [17] employed MoM through a linear approximation of the waveguide boundaries, where these boundaries were divided into segments. Additionally, MoM was also applied at the center of each segment, aiming to solve systems of linear equations in terms of unknown coefficients.

Recently, in [18], the variational Rayleigh-Ritz method was used to model electromagnetic fields in curved rectangular waveguides with uniform cross-section. Thus, the author developed a variational formulation to solve the Maxwell’s equations in a toroidal coordinate system. The Rayleigh-Ritz method was employed for an eigenvalue and eigenvector problem, through an expansion in rectangular harmonics of a straight waveguide as base functions to model a curved rectangular waveguide.

1.2

Thesis Organization

The rest of this dissertation is organized as follows. In Chapter 2, we introduce the boundary value problem and, using the Point Matching method, we demonstrate a solution to the problem by decomposing the y -component. In this chapter, we analyze the results for this proposed solution and for different values of the curvature radius, where we compare the normalized k_ϕ values in [11] with the normalized k_ζ values found in this work using the point matching method.

In Chapter 3, we solve the problem using the MoM approach, a more practical method that allows for a linear eigenvalue problem. In this section, we also analyze the normalized k_ζ values obtained from the MoM and compare them with the exact solution values in [11].

In Chapter 4, we perform a comparison of the relative errors and simulation times between the two presented methods.

Finally, in Chapter 5, we present the conclusions and suggest future research directions.

2 Point Matching Method

The PMM that will be used in this work as an alternative to solve boundary value problems, makes it possible to find an approximate solution to the Helmholtz equation subject to complex boundary conditions, such as curved waveguides. Furthermore, PMM is an economically attractive technique that can offer significant computational advantages, both in terms of computing time and programming effort. In other words, this method does not require time-consuming auxiliary calculations that consume a lot of memory [14].

Consider the geometry of curved rectangular waveguides with a constant radius of curvature R , as illustrated in Fig. 2.1, where the longitudinal direction refers to the ζ -axis. We use the Cartesian coordinate system (x, y, ζ) to describe this problem. Additionally, it is assumed that the waveguide is filled with a lossless medium (characterized by electric permittivity ϵ and magnetic permeability μ) in the domain $R - a/2 < x < R + a/2$ and $-b/2 < y < +b/2$, and is bounded by a perfect electric conductor (PEC).

2.1 Solution through Decomposition of the y Component

From Maxwell's equations, we can obtain the Helmholtz vector equation

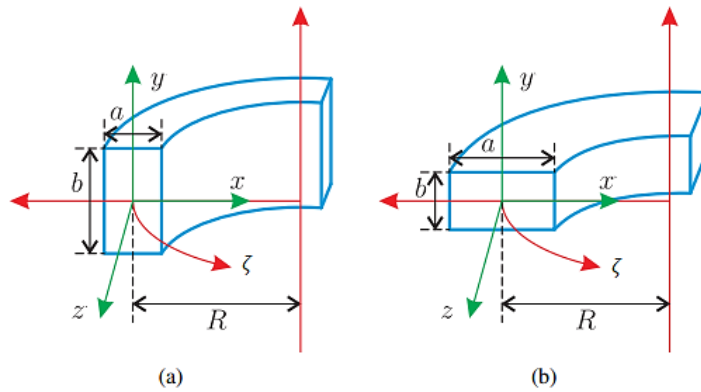


Figure 2.1: Geometry of a rectangular waveguide curved in the (a) E-plane and (b) H-plane.

$$(\nabla^2 + k^2)\vec{F} = \vec{0}, \quad (2-1)$$

in which the fields (electric or magnetic) are represented by the vector $\vec{F} = \{\vec{E}, \vec{H}\}$. The time-harmonic dependence $\exp(+j\omega t)$ is assumed and omitted. In the coordinate system (x, y, ζ) , we have that [19–22]

$$\begin{aligned} \hat{x} \cdot (\nabla^2 + k^2) \vec{F} \\ = (\nabla^2 + k^2) F_x + 2 R^{-1} \frac{1}{h^2} \frac{\partial}{\partial \zeta} F_\zeta - R^{-2} \frac{1}{h^2} F_x, \end{aligned} \quad (2-2)$$

$$\hat{y} \cdot (\nabla^2 + k^2) \vec{F} = (\nabla^2 + k^2) F_y, \quad (2-3)$$

$$\begin{aligned} \hat{\zeta} \cdot (\nabla^2 + k^2) \vec{F} \\ = (\nabla^2 + k^2) F_\zeta - 2 R^{-1} \frac{1}{h^2} \frac{\partial}{\partial x} F_x - R^{-2} \frac{1}{h^2} F_\zeta, \end{aligned} \quad (2-4)$$

where the scalar Laplacian is given by

$$\nabla^2 = \nabla_s^2 + \frac{1}{h^2} \frac{\partial^2}{\partial \zeta^2} - R^{-1} \frac{1}{h} \frac{\partial}{\partial x}, \quad (2-5)$$

with

$$\nabla_s^2 = \frac{\partial^2}{\partial x^2} + \frac{\partial^2}{\partial y^2}. \quad (2-6)$$

The metric coefficient in the curved coordinate is given by [23, 24]

$$h = 1 - R^{-1} x. \quad (2-7)$$

Noting that the y -component is decoupled from the others in (2-2)–(2-4), instead of decomposing the fields in terms of TM and TE contributions for the longitudinal axis ζ , it is more convenient to represent the fields in terms of E_y and H_y due to the decoupling evidenced in (2-3). Thus, after multiplying (2-3) by h^2 , we obtain

$$\left(h^2 \nabla_s^2 + \frac{\partial^2}{\partial \zeta^2} - R^{-1} h \frac{\partial}{\partial x} + h^2 k^2 \right) F_y = 0, \quad (2-8)$$

which can be used to obtain TE^y and TM^y fields with $F_y = H_y$ and $F_y = E_y$, respectively.

Let's expand the fields in terms of planar harmonics, such that

$$E_y = \sum_m a_m \sin \left[k_{xm} \left(x - \frac{a}{2} \right) \right] \times \cos \left[k_{ym} \left(y - \frac{b}{2} \right) \right] e^{-jk_\zeta \zeta}, \quad (2-9)$$

$$H_y = \sum_m a_m \cos \left[k_{xm} \left(x - \frac{a}{2} \right) \right] \times \sin \left[k_{yn} \left(y - \frac{b}{2} \right) \right] e^{-jk_\zeta \zeta}, \quad (2-10)$$

for $\zeta > 0$. The values of k_{xm} and k_{yn} above are the same as those obtained in [2] for the conventional rectangular waveguide, i.e., with a straight longitudinal axis, such that

$$k_{xm} = \frac{m\pi}{a}, m \in \mathbb{Z}, \quad (2-11)$$

$$k_{yn} = \frac{n\pi}{b}, n \in \mathbb{Z}. \quad (2-12)$$

The axial wavenumber is given by $k_\zeta^2 = k^2 h^2 - k_t^2$, com $k = \omega (\epsilon \mu)^{1/2}$, com $\Im m(k_\zeta) \leq 0$ [24, 25]. It is observed that k_t (transverse wavenumber) is not a constant due to the presence of the metric coefficient h . In the scenario where $R \rightarrow \infty$, the axial coordinate $\zeta \rightarrow z$, and the curved rectangular structure recovers the conventional rectangular shape. Thus, we have $k_\zeta \rightarrow k_z = \pm(k^2 - k_{xm}^2 - k_{yn}^2)^{1/2}$. Furthermore, as $h \rightarrow 1$, k_t becomes the radial propagation constant.

Compactly, in view of (2-9) and (2-10), we can write the field component parallel to y to

$$F_y = \bar{f}^T(x) \bar{a} Y(y) e^{-jk_\zeta \zeta}. \quad (2-13)$$

For a point p along x and within the waveguide cross-section, we will use the compact notation

$$\bar{f}_p^T(x) = \bar{f}^T(x = x_p). \quad (2-14)$$

Truncating the series in (2-13) with M harmonics, we can impose that (2-14) is satisfied at $P \geq M$ points along the x domain of the curved waveguide. Due to the presence of $Y(y) e^{-jk_\zeta \zeta}$ in (2-13), we have that the fields of a given mode are invariant in y and ζ along the waveguide. Thus, using $\partial^2/\partial y^2 \rightarrow -k_{yn}^2$ and $\partial^2/\partial \zeta^2 \rightarrow -k_\zeta^2$ in (2-8), we obtain

$$\sum_m \left[h^2 \left(-k_{xm}^2 - k_{yn}^2 \right) - k_\zeta^2 + h^2 k^2 \right] f_{pm} a_m - R^{-1} h k_{xm} \frac{\partial}{\partial (k_{xm} x)} f_{pm} a_m = 0, \quad (2-15)$$

which can be written compactly as

$$\bar{m}_p^T \bar{a} = 0 \quad (2-16)$$

at a given position x_p within the waveguide.

Imposing (2-16) for a set of $p = 1, 2, 3, \dots, P$ points in the domain $-a/2 < x < a/2$, we can write

$$\begin{bmatrix} \bar{m}_1^T \\ \bar{m}_2^T \\ \vdots \\ \bar{m}_P^T \end{bmatrix} \bar{a} = \bar{0}, \quad (2-17)$$

or

$$\bar{M} \bar{a} = \bar{0}. \quad (2-18)$$

The above equation has a non-trivial solution only when

$$\det(\bar{M}) = 0, \quad (2-19)$$

which will provide the eigenvalues k_ζ that solve the problem at hand. For each eigenvalue found by tracking the zeros of $\det(\bar{M})$, the corresponding eigenvector will be given by solving the homogeneous system of equations in (2-18), that is, $\bar{a} = \text{null}(\bar{M})$.

In view of the above, the matrix \bar{M} is filled as follows:

$$\begin{aligned} \bar{M} |_{p,m} = & \\ & \left[h^2 \left(-k_{xm}^2 - k_{yn}^2 \right) - k_\zeta^2 + h^2 k^2 \right] \sin \left[k_{xm} \left(x_p - \frac{a}{2} \right) \right] \\ & - R^{-1} h(k_{xm}) \cos \left[k_{xm} \left(x_p - \frac{a}{2} \right) \right] \end{aligned} \quad (2-20)$$

for TM^y fields, and

$$\begin{aligned} \bar{M} |_{p,m} = & \\ & \left[h^2 \left(-k_{xm}^2 - k_{yn}^2 \right) - k_\zeta^2 + h^2 k^2 \right] \cos \left[k_{xm} \left(x_p - \frac{a}{2} \right) \right] \\ & + R^{-1} h(k_{xm}) \sin \left[k_{xm} \left(x_p - \frac{a}{2} \right) \right] \end{aligned} \quad (2-21)$$

for TE^y fields. We have $m = 1, 2, 3, \dots, M$ and $n = 0, 1, 2, \dots$ for the TM^y configuration, while $m = 0, 1, 2, \dots, M - 1$ and $n = 1, 2, 3, \dots$ for the TE^y configuration.

2.2

Numerical Results

2.2.1

H-Plane with $R = 2a$

Let's consider the problem of a hollow waveguide with a cross-section of $a = 22.86$ mm by $b = 10.16$ mm, operating at a frequency of $f = 10$ GHz, in a scenario where the curvature radius is given by $R = 2a$. In the following examples, we use $P = M = 20$ points on the cross-sectional surface of the

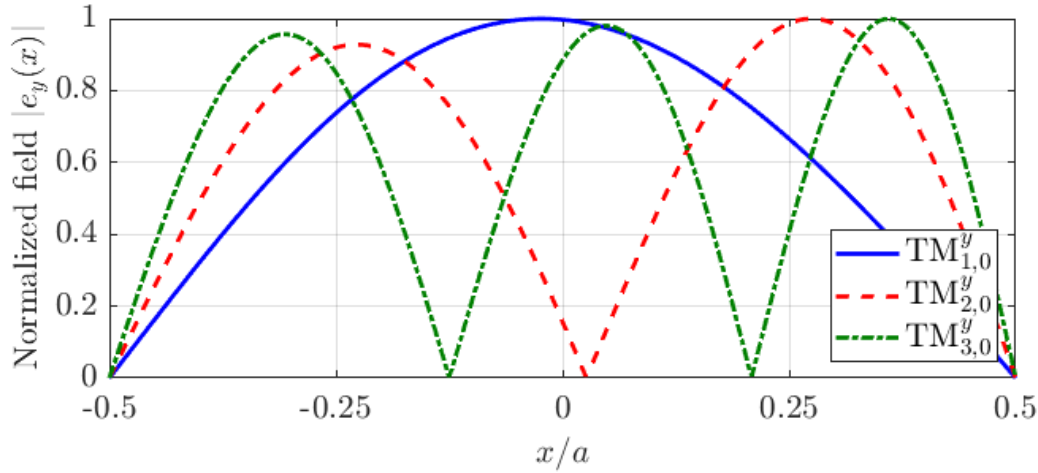


Figure 2.2: Normalized fields $|e_y(x)|$ for the $\text{TM}_{1,0}^y$, $\text{TM}_{2,0}^y$ and $\text{TM}_{3,0}^y$ modes, for $a > b$, $R = 2a$ and $P = 20$ points.

Table 2.1: Normalized longitudinal wavenumbers k_ϕ/k and k_ζ/k for TM modes in a rectangular waveguide curved in the H-plane (with $R = 2a$) obtained respectively by the exact solution (using Bessel functions) in [11] and by our point matching method.

| Mode | k_ϕ/k [11] | Our method (k_ζ/k) | Relative error (%) |
|--------------------|-----------------|----------------------------|--------------------|
| $\text{TM}_{1,0}$ | 0,75297 | 0,75298 | 0,0013372 |
| $\text{TM}_{2,0}$ | $-j$ 0,82630 | $-j$ 0,82645 | 0,017906 |
| $\text{TM}_{3,0}$ | $-j$ 1,6541 | $-j$ 1,6543 | 0,013433 |
| $\text{TM}_{4,0}$ | $-j$ 2,3699 | $-j$ 2,3702 | 0,013651 |
| $\text{TM}_{5,0}$ | $-j$ 3,0532 | $-j$ 3,0537 | 0,014905 |
| $\text{TM}_{6,0}$ | $-j$ 3,7219 | $-j$ 3,7226 | 0,016947 |
| $\text{TM}_{7,0}$ | $-j$ 4,3826 | $-j$ 4,3835 | 0,019919 |
| $\text{TM}_{8,0}$ | $-j$ 5,0384 | $-j$ 5,0397 | 0,024146 |
| $\text{TM}_{9,0}$ | $-j$ 5,6911 | $-j$ 5,6928 | 0,030275 |
| $\text{TM}_{10,0}$ | $-j$ 6,3415 | $-j$ 6,3440 | 0,039387 |

curved rectangular waveguide in the numerical implementation of the proposed PMM.

The normalized fields $|e_y(x)|$ for the $\text{TM}_{1,0}^y$, $\text{TM}_{2,0}^y$ and $\text{TM}_{3,0}^y$ modes obtained with the help of MATLAB in [26] are shown in the Fig. 2.2. The first ten normalized longitudinal wave numbers for the $\text{TM}_{m,0}$ modes resulting from the presented PPM (k_ζ/k) are listed in Table 2.1 and compared with the exact solution obtained in [11]. We find that the field distribution is nearly identical to that of the straight waveguide, with slight deviations in the fundamental mode field, whose maximum shifts subtly from the center to the periphery of the waveguide. The relative error of the eigenvalue compared to the exact solution is less than 0,5%.

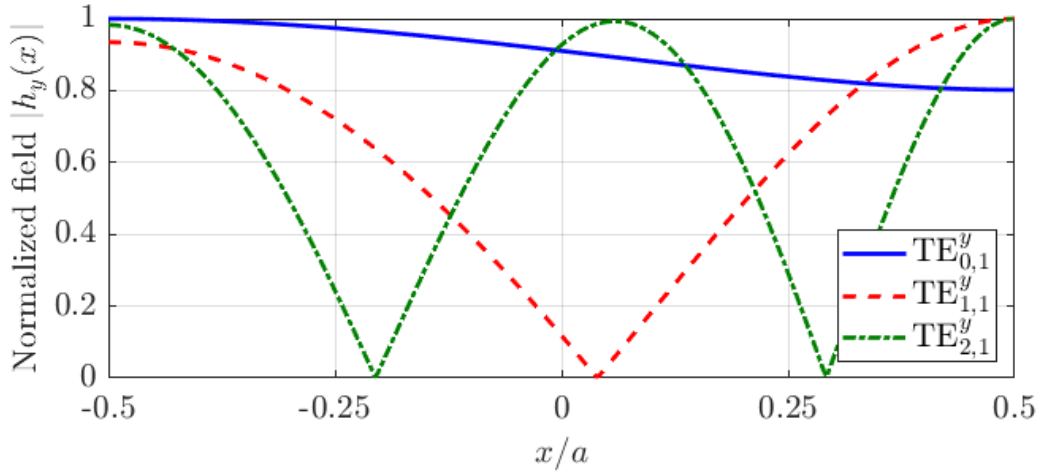


Figure 2.3: Normalized fields $|h_y(x)|$ for the $\text{TE}_{0,1}^y$, $\text{TE}_{1,1}^y$ and $\text{TE}_{2,1}^y$ modes, for $a < b$, $R = 2a$ and $P = 20$ points.

2.2.2

E-Plane with $R = 2a$

Now, we consider a rectangular waveguide curved in the E plane with $a = 10,16$ mm and $b = 22,86$ mm. The parameters f , R and P are the same as in the previous example. The normalized fields $|h_y(x)|$ for the $\text{TE}_{0,1}^y$, $\text{TE}_{1,1}^y$, and $\text{TE}_{2,1}^y$ modes are shown in Fig. 2.3. It is noteworthy that the fundamental mode of the curved waveguide does not have a constant field along x , as in the version for $R \rightarrow \infty$. The lack of symmetry along the x domain due to the curvature becomes evident by observing the positions of the maximum and null of the $\text{TE}_{1,1}^y$ and $\text{TE}_{2,1}^y$ fields. The first ten normalized longitudinal wavenumbers for the $\text{TE}_{m,1}$ modes obtained by the PMM (k_ζ/k) are shown in Table 2.2, and we again observe good agreement with the exact solution.

2.2.3

H-Plane with $R = a$

For the H plane, the curves of $|e_y(x)|$ for the $\text{TM}_{1,0}^y$, $\text{TM}_{2,0}^y$ and $\text{TM}_{3,0}^y$ modes are illustrated in Fig. 2.4, and the values for (k_ζ/k) are shown in Table 2.3. The effects of the finite curvature radius become more pronounced, and the loss of symmetry along the x domain becomes significant compared to the well-known solution for $R \rightarrow \infty$. Regarding the eigenvalues, good agreement is observed with the exact solution.

2.2.4

E-Plane with $R = a$

For the E plane, the curves of $|h_y(x)|$ for the $\text{TE}_{0,1}^y$, $\text{TE}_{1,1}^y$, and $\text{TE}_{2,1}^y$ modes obtained are shown in Fig. 2.5, and the values of (k_ζ/k) are displayed

Table 2.2: Normalized longitudinal wavenumbers k_ϕ/k and k_ζ/k for TE modes in a rectangular waveguide curved in the E-plane (with $R = 2a$) obtained respectively by the exact solution (using Bessel functions) in [11] and by our point matching method.

| Mode | k_ϕ/k [11] | Our method (k_ζ/k) | Relative error (%) |
|-------------------|-----------------|----------------------------|--------------------|
| TE _{0,1} | 0,75527 | 0,75544 | 0,021483 |
| TE _{1,1} | $-j$ 1,2340 | $-j$ 1,2349 | 0,072729 |
| TE _{2,1} | $-j$ 2,7895 | $-j$ 2,7914 | 0,069034 |
| TE _{3,1} | $-j$ 4,2673 | $-j$ 4,2703 | 0,070585 |
| TE _{4,1} | $-j$ 5,7278 | $-j$ 5,7323 | 0,078709 |
| TE _{5,1} | $-j$ 7,1817 | $-j$ 7,1878 | 0,085480 |
| TE _{6,1} | $-j$ 8,6323 | $-j$ 8,6411 | 0,10225 |
| TE _{7,1} | $-j$ 10,081 | $-j$ 10,093 | 0,11575 |
| TE _{8,1} | $-j$ 11,529 | $-j$ 11,546 | 0,15059 |
| TE _{9,1} | $-j$ 12,975 | $-j$ 12,998 | 0,17574 |

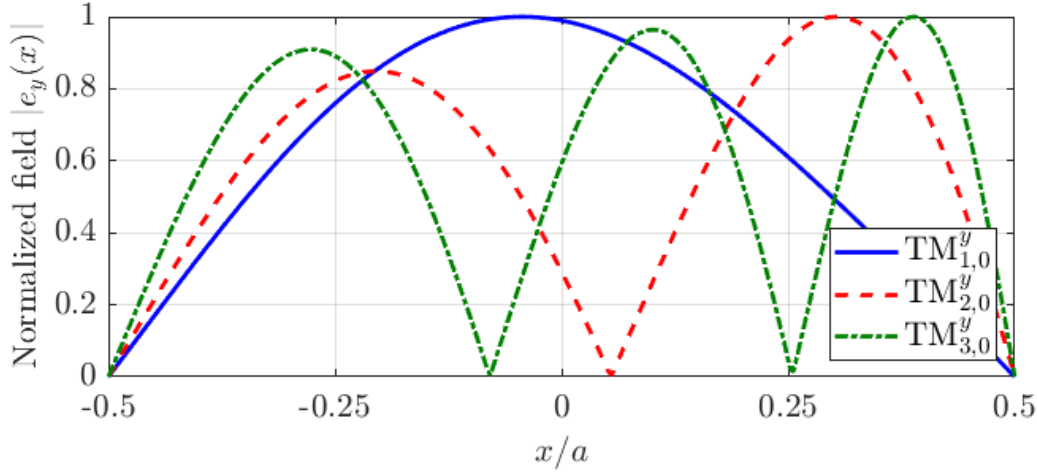


Figure 2.4: Normalized fields $|e_y(x)|$ for the $\text{TM}_{1,0}^y$, $\text{TM}_{2,0}^y$ and $\text{TM}_{3,0}^y$ modes, for $a > b$, $R = a$ and $P = 20$ points.

in Table 2.4. Again, relatively good agreement is observed with the reference exact solution. In this case, the effects of the finite curvature radius intensify and cause the fundamental mode field to concentrate on the outer periphery (pointing in the opposite direction of the curvature center) of the waveguide.

2.2.5

H-Plane with $R = 0.75a$

In this scenario, for the H plane, the curves of $|e_y(x)|$ for the $\text{TM}_{1,0}^y$, $\text{TM}_{2,0}^y$ and $\text{TM}_{3,0}^y$ modes are illustrated in Fig. 2.6, and the values for (k_ζ/k) are shown in Table 2.5. We again observe the effects of the finite curvature radius and the good agreement of the obtained eigenvalues in relation to the exact solution eigenvalues.

Table 2.3: Normalized longitudinal wavenumbers k_ϕ/k and k_ζ/k for TM modes in a rectangular waveguide curved in the H-plane (with $R = a$) obtained respectively by the exact solution (using Bessel functions) in [11] and by our point matching method.

| Mode | k_ϕ/k [11] | Our method (k_ζ/k) | Relative error (%) |
|--------------------|-----------------|----------------------------|--------------------|
| TM _{1,0} | 0,74677 | 0,74682 | 0,0060834 |
| TM _{2,0} | $-j$ 0,75520 | $-j$ 0,75597 | 0,10114 |
| TM _{3,0} | $-j$ 1,5250 | $-j$ 1,5262 | 0,080599 |
| TM _{4,0} | $-j$ 2,1926 | $-j$ 2,1945 | 0,086194 |
| TM _{5,0} | $-j$ 2,8298 | $-j$ 2,8326 | 0,10039 |
| TM _{6,0} | $-j$ 3,4530 | $-j$ 3,4572 | 0,12392 |
| TM _{7,0} | $-j$ 4,0684 | $-j$ 4,0750 | 0,16174 |
| TM _{8,0} | $-j$ 4,6791 | $-j$ 4,6896 | 0,22368 |
| TM _{9,0} | $-j$ 5,2867 | $-j$ 5,3041 | 0,33048 |
| TM _{10,0} | $-j$ 5,8921 | $-j$ 5,9227 | 0,52018 |

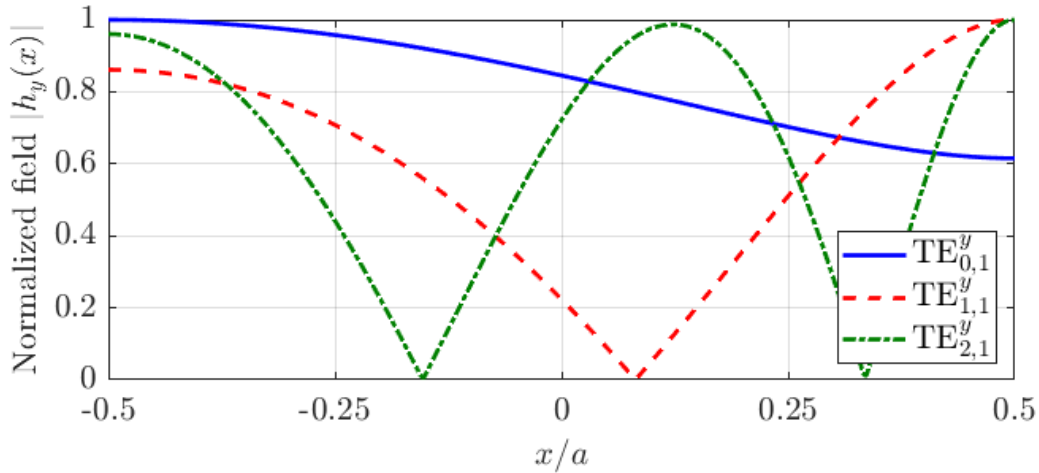


Figure 2.5: Normalized fields $|h_y(x)|$ for the $\text{TE}_{0,1}^y$, $\text{TE}_{1,1}^y$, and $\text{TE}_{2,1}^y$ modes, for $a < b$, $R = a$ and $P = 20$ points.

2.2.6

E-Plane with $R = 0.75a$

For the E plane, the curves of $|h_y(x)|$ for the $\text{TE}_{0,1}^y$, $\text{TE}_{1,1}^y$, and $\text{TE}_{2,1}^y$ modes obtained are shown in Fig. 2.7, and the values of (k_ζ/k) are displayed in Table 2.6. Once again, the obtained values are in agreement with the exact solution.

2.2.7

H-Plane with $R = 10a$

In this scenario, for the H plane, the curves of $|e_y(x)|$ for the $\text{TM}_{1,0}^y$, $\text{TM}_{2,0}^y$ and $\text{TM}_{3,0}^y$ modes are illustrated in Fig. 2.8, and the values for (k_ζ/k) are shown in Table 2.7. For this case, we note that the values we obtained are

Table 2.4: Normalized longitudinal wavenumbers k_ϕ/k and k_ζ/k for TE modes in a rectangular waveguide curved in the E-plane (with $R = a$) obtained respectively by the exact solution (using Bessel functions) in [11] and by our point matching method.

| Mode | k_ϕ/k [11] | Our method (k_ζ/k) | Relative error (%) |
|-------------------|-----------------|----------------------------|--------------------|
| TE _{0,1} | 0,75607 | 0,75685 | 0,10267 |
| TE _{1,1} | $-j$ 1,1262 | $-j$ 1,1310 | 0,42648 |
| TE _{2,1} | $-j$ 2,5856 | $-j$ 2,5962 | 0,40852 |
| TE _{3,1} | $-j$ 3,9633 | $-j$ 3,9801 | 0,42396 |
| TE _{4,1} | $-j$ 5,3229 | $-j$ 5,3498 | 0,50453 |
| TE _{5,1} | $-j$ 6,6757 | $-j$ 6,7133 | 0,56193 |
| TE _{6,1} | $-j$ 8,0252 | $-j$ 8,0858 | 0,75467 |
| TE _{7,1} | $-j$ 9,3728 | $-j$ 9,4530 | 0,85590 |
| TE _{8,1} | $-j$ 10,719 | $-j$ 10,862 | 1,3359 |
| TE _{9,1} | $-j$ 12,065 | $-j$ 12,236 | 1,4169 |

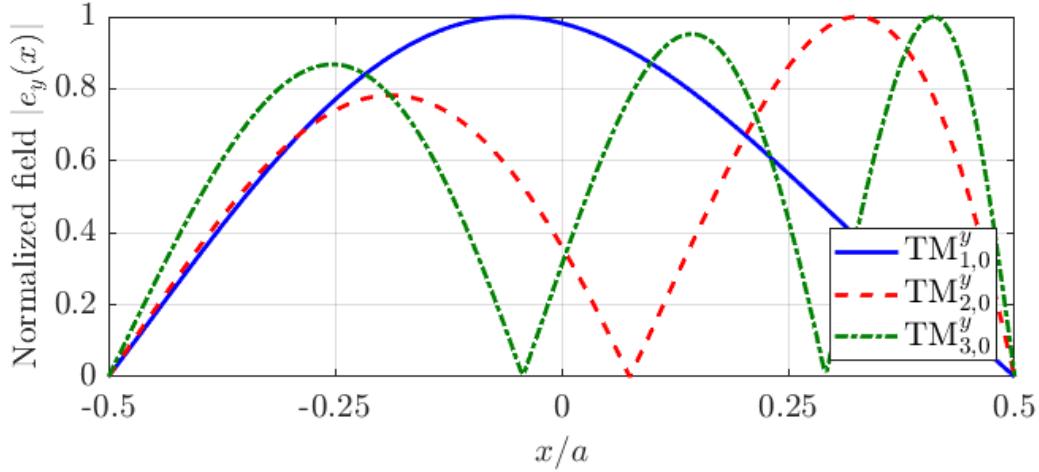


Figure 2.6: Normalized fields $|e_y(x)|$ for the $\text{TM}_{1,0}^y$, $\text{TM}_{2,0}^y$ and $\text{TM}_{3,0}^y$ modes, for $a > b$, $R = 0.75a$ and $P = 20$ points.

much closer to the exact solution compared to the other cases. In other words, the values of the relative error for $R = 10a$ are much smaller.

2.2.8

E-Plane with $R = 10a$

For the E plane, the curves of $|h_y(x)|$ for the $\text{TE}_{0,1}^y$, $\text{TE}_{1,1}^y$, and $\text{TE}_{2,1}^y$ modes obtained are shown in Fig. 2.9, and the values of (k_ζ/k) are displayed in Table 2.8. Again, the obtained values are very close to the exact solution.

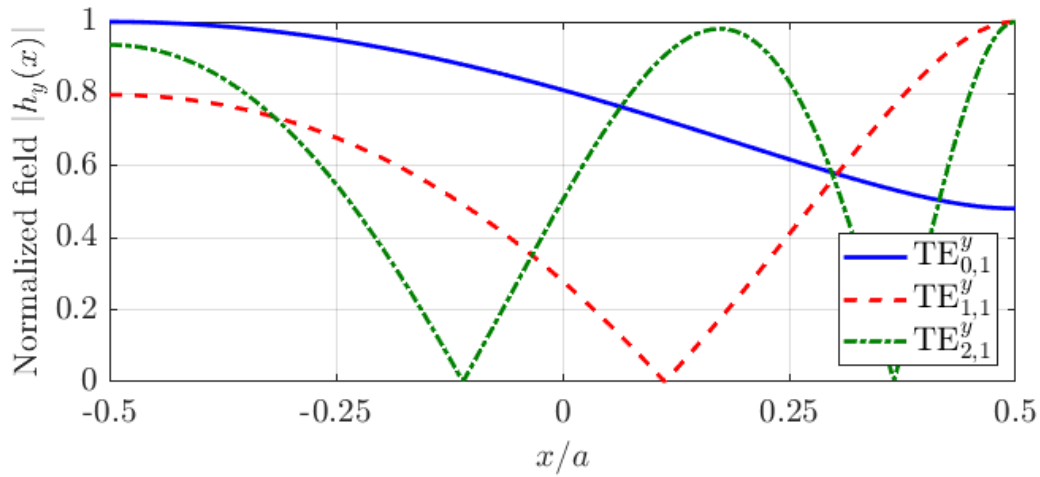


Figure 2.7: Normalized fields $|h_y(x)|$ for the $TE_{0,1}^y$, $TE_{1,1}^y$ and $TE_{2,1}^y$ modes, for $a < b$, $R = 0.75a$ and $P = 20$ points.

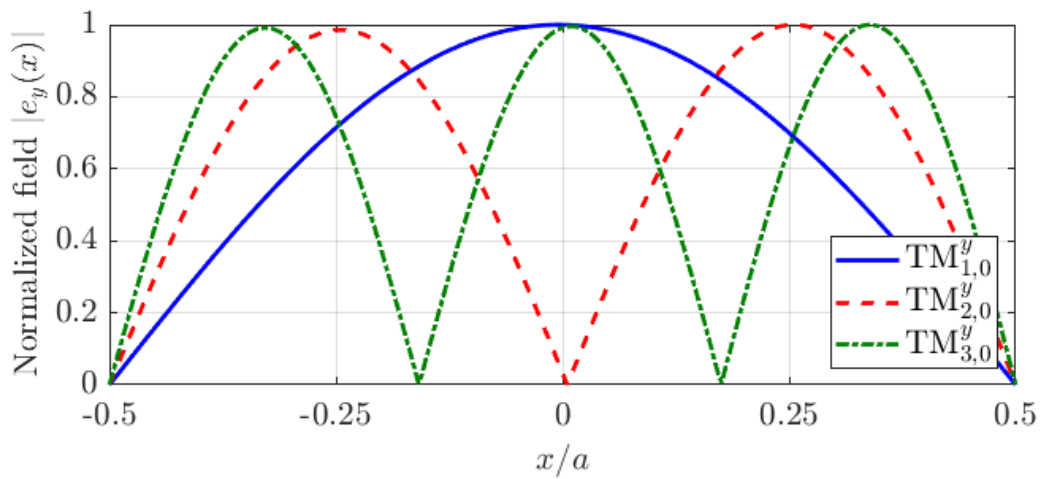


Figure 2.8: Normalized fields $|e_y(x)|$ for the $TM_{1,0}^y$, $TM_{2,0}^y$ and $TM_{3,0}^y$ modes, for $a > b$, $R = 10a$ and $P = 20$ points.

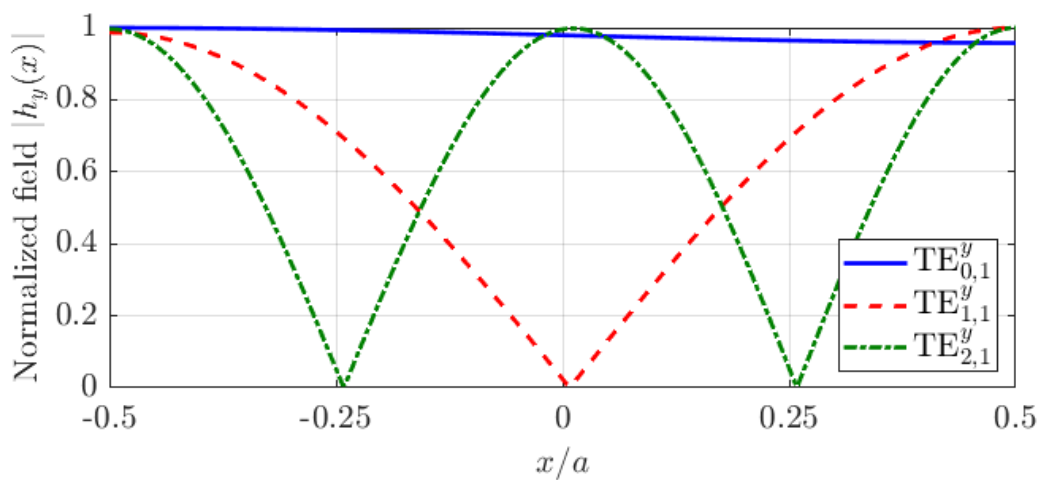


Figure 2.9: Normalized fields $|h_y(x)|$ for the $TE_{0,1}^y$, $TE_{1,1}^y$ and $TE_{2,1}^y$ modes, for $a < b$, $R = 10a$ and $P = 20$ points.

Table 2.5: Normalized longitudinal wavenumbers k_ϕ/k and k_ζ/k for TM modes in a rectangular waveguide curved in the H-plane (with $R = 0.75a$) obtained respectively by the exact solution (using Bessel functions) in [11] and by our point matching method.

| Mode | k_ϕ/k [11] | Our method (k_ζ/k) | Relative error (%) |
|--------------------|-----------------|----------------------------|--------------------|
| TM _{1,0} | 0,74023 | 0,74032 | 0,012558 |
| TM _{2,0} | $-j$ 0,67168 | $-j$ 0,67361 | 0,28627 |
| TM _{3,0} | $-j$ 1,3716 | $-j$ 1,3750 | 0,25043 |
| TM _{4,0} | $-j$ 1,9816 | $-j$ 1,9873 | 0,29150 |
| TM _{5,0} | $-j$ 2,5635 | $-j$ 2,5732 | 0,37747 |
| TM _{6,0} | $-j$ 3,1323 | $-j$ 3,1489 | 0,52912 |
| TM _{7,0} | $-j$ 3,6937 | $-j$ 3,7230 | 0,79451 |
| TM _{8,0} | $-j$ 4,2505 | $-j$ 4,3037 | 1,2498 |
| TM _{9,0} | $-j$ 4,8043 | $-j$ 4,9005 | 2,0005 |
| TM _{10,0} | $-j$ 5,3560 | $-j$ 5,5244 | 3,1445 |

Table 2.6: Normalized longitudinal wavenumbers k_ϕ/k and k_ζ/k for TE modes in a rectangular waveguide curved in the E-plane (with $R = 0.75a$) obtained respectively by the exact solution (using Bessel functions) in [11] and by our point matching method.

| Mode | k_ϕ/k [11] | Our method (k_ζ/k) | Relative error (%) |
|-------------------|-----------------|----------------------------|--------------------|
| TE _{0,1} | 0,75707 | 0,75880 | 0,22753 |
| TE _{1,1} | $-j$ 0,99887 | $-j$ 1,0113 | 1,2424 |
| TE _{2,1} | $-j$ 2,3425 | $-j$ 2,3710 | 1,2146 |
| TE _{3,1} | $-j$ 3,6006 | $-j$ 3,6466 | 1,2786 |
| TE _{4,1} | $-j$ 4,8399 | $-j$ 4,9202 | 1,6587 |
| TE _{5,1} | $-j$ 6,0722 | $-j$ 6,1839 | 1,8394 |
| TE _{6,1} | $-j$ 7,3011 | $-j$ 7,5034 | 2,7714 |
| TE _{7,1} | $-j$ 8,5280 | $-j$ 8,7743 | 2,8873 |
| TE _{8,1} | $-j$ 9,7538 | $-j$ 10,249 | 5,0820 |
| TE _{9,1} | $-j$ 10,979 | $-j$ 11,468 | 4,4578 |

Table 2.7: Normalized longitudinal wavenumbers k_ϕ/k and k_ζ/k for TM modes in a rectangular waveguide curved in the H-plane (with $R = 10a$) obtained respectively by the exact solution (using Bessel functions) in [11] and by our point matching method.

| Mode | k_ϕ/k [11] | Our method (k_ζ/k) | Relative error (%) |
|--------------------|-----------------|----------------------------|--------------------|
| TM _{1,0} | 0,75493 | 0,75493 | 0,000051473 |
| TM _{2,0} | $-j$ 0,84756 | $-j$ 0,84757 | 0,00065091 |
| TM _{3,0} | $-j$ 1,6924 | $-j$ 1,6924 | 0,00048084 |
| TM _{4,0} | $-j$ 2,4226 | $-j$ 2,4226 | 0,00048265 |
| TM _{5,0} | $-j$ 3,1196 | $-j$ 3,1196 | 0,00051900 |
| TM _{6,0} | $-j$ 3,8018 | $-j$ 3,8018 | 0,00057881 |
| TM _{7,0} | $-j$ 4,4759 | $-j$ 4,4759 | 0,00066396 |
| TM _{8,0} | $-j$ 5,1451 | $-j$ 5,1452 | 0,00078058 |
| TM _{9,0} | $-j$ 5,8112 | $-j$ 5,8112 | 0,00094084 |
| TM _{10,0} | $-j$ 6,4750 | $-j$ 6,4750 | 0,0011629 |

Table 2.8: Normalized longitudinal wavenumbers k_ϕ/k and k_ζ/k for TE modes in a rectangular waveguide curved in the E-plane (with $R = 10a$) obtained respectively by the exact solution (using Bessel functions) in [11] and by our point matching method.

| Mode | k_ϕ/k [11] | Our method (k_ζ/k) | Relative error (%) |
|-------------------|-----------------|----------------------------|--------------------|
| TE _{0,1} | 0,75502 | 0,75503 | 0,00081668 |
| TE _{1,1} | $-j$ 1,2662 | $-j$ 1,2662 | 0,0026113 |
| TE _{2,1} | $-j$ 2,8500 | $-j$ 2,8501 | 0,0024758 |
| TE _{3,1} | $-j$ 4,3575 | $-j$ 4,3576 | 0,0025212 |
| TE _{4,1} | $-j$ 5,8480 | $-j$ 5,8482 | 0,0027670 |
| TE _{5,1} | $-j$ 7,3319 | $-j$ 7,3321 | 0,0029775 |
| TE _{6,1} | $-j$ 8,8125 | $-j$ 8,8128 | 0,0034578 |
| TE _{7,1} | $-j$ 10,291 | $-j$ 10,292 | 0,0038693 |
| TE _{8,1} | $-j$ 11,769 | $-j$ 11,769 | 0,0047711 |
| TE _{9,1} | $-j$ 13,246 | $-j$ 13,246 | 0,0055322 |

3 Method of Moments

The Method of Moments is a technique used to solve surface or volume electromagnetic integral equations in the frequency domain. In other words, in summary, it is a technique that converts integral equations into a linear system, which can be easily solved numerically via computer. Additionally, this method is widely used in solving radiation and scattering problems [27].

The non-homogeneous equation is considered [27–29]

$$L(f) = g \quad (3-1)$$

where L is a linear operator, g is the source or excitation (known function), and f is the field or response (unknown function that needs to be determined).

Expanding f into a sum of N weighted basis functions, we have

$$f = \sum_{n=1}^N a_n f_n \quad (3-2)$$

where a_n are unknown coefficients. Substituting (3-2) into (3-1) and using the linearity of L , we obtain

$$\sum_{n=1}^N a_n L(f_n) = g \quad (3-3)$$

Assuming an inner product $\langle f, g \rangle$. Now, defining a set of weight functions w_1, w_2, w_3, \dots in the domain of L , and associating the inner product of (3-3) with each w_m , we have

$$\sum_{n=1}^N a_n \langle w_m, Lf_n \rangle = \langle w_m, g \rangle, \quad m = 1, 2, 3, \dots \quad (3-4)$$

In matrix form, we can write (3-4) as

$$\bar{\bar{M}}_{mn} \bar{a}_n = \bar{g}_m \quad (3-5)$$

where

$$\bar{\bar{M}}_{mn} = \begin{bmatrix} \langle w_1, Lf_1 \rangle & \langle w_1, Lf_2 \rangle & \dots \\ \langle w_2, Lf_1 \rangle & \langle w_2, Lf_2 \rangle & \dots \\ \dots & \dots & \dots \end{bmatrix} \quad (3-6)$$

$$\bar{a}_n = \begin{bmatrix} a_1 \\ a_2 \\ \vdots \end{bmatrix} \quad (3-7)$$

$$\bar{g}_m = \begin{bmatrix} \langle w_1, g \rangle \\ \langle w_2, g \rangle \\ \vdots \end{bmatrix} \quad (3-8)$$

If the matrix \bar{M} is nonsingular, its inverse \bar{M}^{-1} exists. Thus, the coefficients \bar{a}_n are given by

$$\bar{a}_n = \left(\bar{M}_{mn} \right)^{-1} \bar{g}_m \quad (3-9)$$

and the solution for f is given by (3-2). For a precise expression of this result, the matrix of functions is defined as

$$\bar{f} = [f_1 \ f_2 \ f_3 \ \dots] \quad (3-10)$$

and we obtain

$$f = \bar{f} \bar{a}_n = \bar{f} \left(\bar{M}_{mn} \right)^{-1} \bar{g}_m \quad (3-11)$$

3.1 Solution of the Linear Eigenvalue Problem

We can rewrite (2-8) as

$$\left(L - k_\zeta^2 \right) F_y = 0, \quad (3-12)$$

where L is the differential operator defined as

$$L = h^2 \nabla_s^2 - R^{-1} h \frac{\partial}{\partial x} + h^2 k^2 = h^2 \left(\frac{\partial^2}{\partial x^2} + \frac{\partial^2}{\partial y^2} \right) - R^{-1} h \frac{\partial}{\partial x} + h^2 k^2 \quad (3-13)$$

and $\partial^2 / \partial \zeta^2 = -k_\zeta^2$.

Rewriting (3-12), we have

$$\left(L - k_\zeta^2 \right) \bar{f}^T \bar{a} = 0. \quad (3-14)$$

Therefore, we expand f as in (3-2) to solve for the unknowns \bar{a} by calculating integrals of each differential equation over the transverse surface of the curved waveguide. To do this, we test with the weighting function w_p and take the surface integral

$$\int_S w_p \left(L - k_\zeta^2 \right) \bar{f}^T \bar{a} dS = 0, \quad \forall p = 1, 2, 3, \dots, P. \quad (3-15)$$

For the point matching method, it is assumed

$$w_p = \delta(x - x_p) \delta(y - y_p). \quad (3-16)$$

Writing in matrix form, we have for $p = 1$

$$\left[\langle w_1, L\bar{f}^T \rangle_S - k_\zeta^2 \langle w_1, \bar{f}^T \rangle_S \right] \bar{a} = 0. \quad (3-17)$$

Stacking all the P equations, we can write

$$\bar{\bar{M}} \bar{a} = 0 \quad (3-18)$$

where

$$\bar{\bar{M}} = \begin{bmatrix} \langle w_1, L\bar{f}^T \rangle_S - k_\zeta^2 \langle w_1, \bar{f}^T \rangle_S \\ \langle w_2, L\bar{f}^T \rangle_S - k_\zeta^2 \langle w_2, \bar{f}^T \rangle_S \\ \vdots \\ \langle w_p, L\bar{f}^T \rangle_S - k_\zeta^2 \langle w_p, \bar{f}^T \rangle_S \end{bmatrix} \quad (3-19)$$

Compactly, (3-19) can be written as

$$\bar{\bar{M}} = (\bar{\bar{M}}_1 - k_\zeta^2 \bar{\bar{M}}_2) \quad (3-20)$$

Thus, we rewrite (3-18) as follows:

$$(\bar{\bar{M}}_1 - k_\zeta^2 \bar{\bar{M}}_2) \bar{a} = 0 \quad (3-21)$$

where

$$\bar{\bar{M}}_1 |_{p,m} = \langle w_p, L\bar{f} |_m \rangle_S \quad (3-22)$$

$$\bar{\bar{M}}_2 |_{p,m} = \langle w_p, \bar{f} |_m \rangle_S \quad (3-23)$$

Using (3-16), we can rewrite (3-22) and (3-23) as

$$\bar{\bar{M}}_1 |_{p,m} = L\bar{f} |_m (x_p, y_p) \quad (3-24)$$

$$\bar{\bar{M}}_2 |_{p,m} = \bar{f} |_m (x_p, y_p) \quad (3-25)$$

Instead of imposing boundary conditions at discrete points, as we did in the point matching method, we will impose the boundary conditions over the entire problem domain. One of the most common methods is the Galerkin Method, where the basis functions are used as test functions, i.e., $f = g$. Choosing this particular case, we have $w_p = f_p$. Thus, we assume

$$w_p = f_p = \sin \left(k_{xp} \left(x - \frac{a}{2} \right) \right) \quad (3-26)$$

for TM^y fields, and

$$w_p = f_p = \cos \left(k_{xp} \left(x - \frac{a}{2} \right) \right) \quad (3-27)$$

Table 3.1: Normalized longitudinal wavenumbers k_ϕ/k and k_ζ/k for TM modes in a rectangular waveguide curved in the H-plane (with $R = 2a$) obtained respectively by the exact solution (using Bessel functions) in [11] and by the method of moments.

| Mode | k_ϕ/k [11] | Our method (k_ζ/k) | Relative error (%) |
|--------------------|-----------------|----------------------------|--------------------|
| TM _{1,0} | 0,75297 | 0,75297 | 0,000087244 |
| TM _{2,0} | $-j$ 0,82630 | $-j$ 0,82630 | 0,00042928 |
| TM _{3,0} | $-j$ 1,6541 | $-j$ 1,6541 | 0,00024803 |
| TM _{4,0} | $-j$ 2,3699 | $-j$ 2,3699 | 0,00028264 |
| TM _{5,0} | $-j$ 3,0532 | $-j$ 3,0533 | 0,00028550 |
| TM _{6,0} | $-j$ 3,7219 | $-j$ 3,7219 | 0,00039606 |
| TM _{7,0} | $-j$ 4,3826 | $-j$ 4,3826 | 0,00046152 |
| TM _{8,0} | $-j$ 5,0384 | $-j$ 5,0385 | 0,00073781 |
| TM _{9,0} | $-j$ 5,6911 | $-j$ 5,6911 | 0,0010089 |
| TM _{10,0} | $-j$ 6,3415 | $-j$ 6,3416 | 0,0019192 |

for TE^y fields.

Using (3-26), we can rewrite (3-22) and (3-23) as

$$\bar{M}_1|_{p,m} = \int \sin\left(k_{xp}\left(x - \frac{a}{2}\right)\right) L\bar{f}_m(x, y) dS \quad (3-28)$$

$$\bar{M}_2|_{p,m} = \int \sin\left(k_{xp}\left(x - \frac{a}{2}\right)\right) \bar{f}_m(x, y) dS \quad (3-29)$$

Using (3-27), we can rewrite (3-22) and (3-23) as

$$\bar{M}_1|_{p,m} = \int \cos\left(k_{xp}\left(x - \frac{a}{2}\right)\right) L\bar{f}_m(x, y) dS \quad (3-30)$$

$$\bar{M}_2|_{p,m} = \int \cos\left(k_{xp}\left(x - \frac{a}{2}\right)\right) \bar{f}_m(x, y) dS \quad (3-31)$$

3.2

Numerical Results

3.2.1

H-Plane with $R = 2a$

Using the same parameters as in the H-plane scenario for the point matching method, we have the first ten normalized longitudinal wavenumbers for the TM_{*m*,0} modes resulting from the method of moments (k_ζ/k), as shown in Table 3.1. The curves of $|e_y(x)|$ for the TM_{1,0}^y, TM_{2,0}^y and TM_{3,0}^y modes are very similar to those shown in Fig. 2.2, meaning that the relative errors between these curves for these two methods are quite small. It is observed that the relative error of the eigenvalue compared to the exact solution is less than 0,005%.

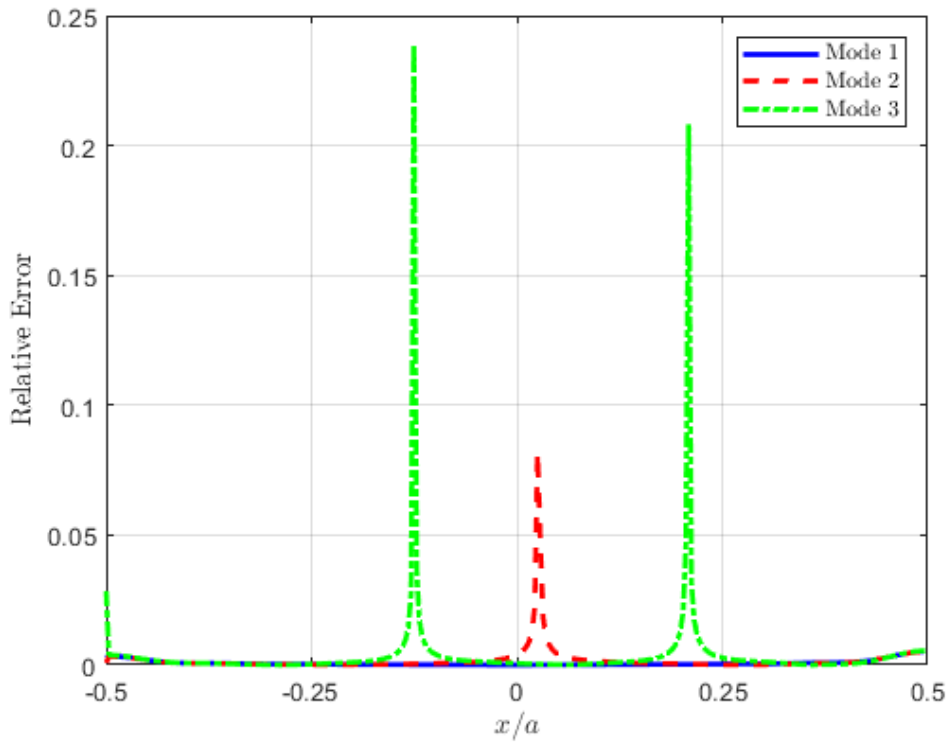


Figure 3.1: Relative error (%) of the normalized field curves $|e_y(x)|$ between PMM and MoM for $\text{TM}_{1,0}^y$, $\text{TM}_{2,0}^y$ and $\text{TM}_{3,0}^y$ modes, for $a > b$, $R = 2a$ and $P = 20$ points.

We note that the normalized field curves are very similar for the two methods presented. Thus, we plotted the relative error of these curves between the methods and observed that the errors for the fundamental mode are practically negligible. Furthermore, for the second mode, the errors are very low, below 0,1. For the third mode, the errors are below 0,25. Therefore, the PMM and MoM methods are in good agreement.

3.2.2

E-Plane with $R = 2a$

Using the same parameters as in the E-plane scenario for the point matching method, we have the first ten normalized longitudinal wavenumbers for the $\text{TE}_{m,1}$ modes resulting from the method of moments (k_ζ/k), as shown in Table 3.2. The curves of $|h_y(x)|$ for the $\text{TE}_{0,1}^y$, $\text{TE}_{1,1}^y$, and $\text{TE}_{2,1}^y$ modes are in accordance with the curves in Fig. 2.3. Again, the relative error of the eigenvalue compared to the exact solution is less than 0,005%.

For the E-plane, the relative errors for the fundamental mode are also practically zero. For the second mode, the errors are below 0,6, and for the third mode, they are less than 1,2. Similar to the H-plane, the errors occur

Table 3.2: Normalized longitudinal wavenumbers k_ϕ/k and k_ζ/k for TE modes in a rectangular waveguide curved in the E-plane (with $R = 2a$) obtained respectively by the exact solution (using Bessel functions) in [11] and by the method of moments.

| Mode | k_ϕ/k [11] | Our method (k_ζ/k) | Relative error (%) |
|-------------------|-----------------|----------------------------|--------------------|
| TE _{0,1} | 0,75527 | 0,75527 | 0,000061226 |
| TE _{1,1} | $-j$ 1,2340 | $-j$ 1,2340 | 0,00025089 |
| TE _{2,1} | $-j$ 2,7895 | $-j$ 2,7895 | 0,00021538 |
| TE _{3,1} | $-j$ 4,2673 | $-j$ 4,2673 | 0,00026579 |
| TE _{4,1} | $-j$ 5,7278 | $-j$ 5,7278 | 0,00027317 |
| TE _{5,1} | $-j$ 7,1817 | $-j$ 7,1817 | 0,00037843 |
| TE _{6,1} | $-j$ 8,6323 | $-j$ 8,6323 | 0,00043367 |
| TE _{7,1} | $-j$ 10,081 | $-j$ 10,081 | 0,00068292 |
| TE _{8,1} | $-j$ 11,529 | $-j$ 11,529 | 0,00090683 |
| TE _{9,1} | $-j$ 12,975 | $-j$ 12,976 | 0,0016904 |

Table 3.3: Normalized longitudinal wavenumbers k_ϕ/k and k_ζ/k for TM modes in a rectangular waveguide curved in the H-plane (with $R = a$) obtained respectively by the exact solution (using Bessel functions) in [11] and by the method of moments.

| Mode | k_ϕ/k [11] | Our method (k_ζ/k) | Relative error (%) |
|--------------------|-----------------|----------------------------|--------------------|
| TM _{1,0} | 0,74677 | 0,74677 | 0,00041013 |
| TM _{2,0} | $-j$ 0,75520 | $-j$ 0,75524 | 0,0044792 |
| TM _{3,0} | $-j$ 1,5250 | $-j$ 1,5250 | 0,0033919 |
| TM _{4,0} | $-j$ 2,1926 | $-j$ 2,1927 | 0,0044001 |
| TM _{5,0} | $-j$ 2,8298 | $-j$ 2,8300 | 0,0060072 |
| TM _{6,0} | $-j$ 3,4530 | $-j$ 3,4533 | 0,010240 |
| TM _{7,0} | $-j$ 4,0684 | $-j$ 4,0691 | 0,018223 |
| TM _{8,0} | $-j$ 4,6791 | $-j$ 4,6809 | 0,038765 |
| TM _{9,0} | $-j$ 5,2867 | $-j$ 5,2912 | 0,085774 |
| TM _{10,0} | $-j$ 5,8921 | $-j$ 5,9042 | 0,20585 |

when the normalized fields $|h_y(x)|$ and $|e_y(x)|$ are practically zero.

3.2.3

H-Plane with $R = a$

Table 3.3 shows the first ten normalized longitudinal wavenumbers for the TM _{$m,0$} modes resulting from the method of moments, and we note good agreement with the exact solution. The curves of $|e_y(x)|$ for the TM_{1,0}^y, TM_{2,0}^y and TM_{3,0}^y modes are consistent with the curves in Fig. 2.4.

For this scenario, we observed that the relative error values for the first mode were practically zero, as in the previous case. For the second and third modes, the errors were higher compared to the case of $R = 2a$. Once again,

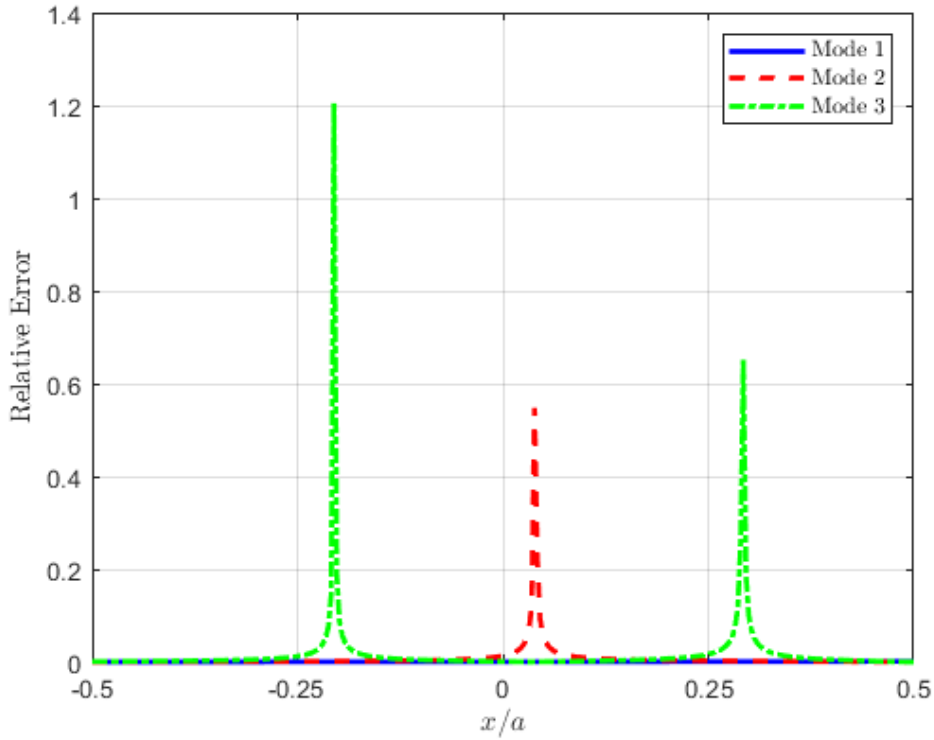


Figure 3.2: Relative error (%) of the normalized field curves $|h_y(x)|$ between PMM and MoM for $\text{TE}_{0,1}^y$, $\text{TE}_{1,1}^y$ and $\text{TE}_{2,1}^y$ modes, for $a > b$, $R = 2a$ and $P = 20$ points.

the errors appear when the normalized fields are nearly zero, that is, when the $\text{TM}_{2,0}^y$ and $\text{TM}_{3,0}^y$ fields are negligible.

3.2.4

E-Plane with $R = a$

For the E-plane, the first ten normalized longitudinal wavenumbers for the $\text{TE}_{m,1}$ modes resulting from the method of moments are shown in Table 3.4, and again we observe good agreement with the exact solution. The curves of $|h_y(x)|$ for the $\text{TE}_{0,1}^y$, $\text{TE}_{1,1}^y$, and $\text{TE}_{2,1}^y$ modes are equivalent to the curves in Fig. 2.5.

For the TE^y modes, the errors for the $\text{TE}_{1,1}^y$ and $\text{TE}_{2,1}^y$ modes were slightly smaller compared to the TM^y modes. In this context, the relative error was higher for the second mode. Furthermore, once again, the errors occur when the fields are nearly zero, and both methods are also in good agreement.

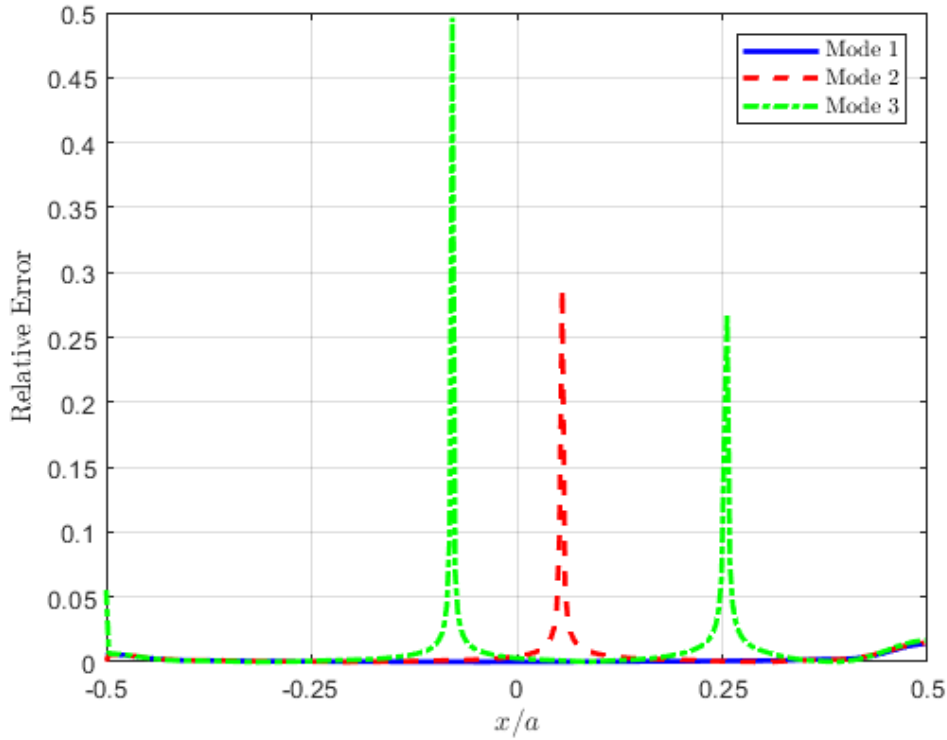


Figure 3.3: Relative error (%) of the normalized field curves $|e_y(x)|$ between PMM and MoM for $\text{TM}_{1,0}^y$, $\text{TM}_{2,0}^y$ and $\text{TM}_{3,0}^y$ modes, for $a > b$, $R = a$ and $P = 20$ points.

Table 3.4: Normalized longitudinal wavenumbers k_ϕ/k and k_ζ/k for TE modes in a rectangular waveguide curved in the E-plane (with $R = a$) obtained respectively by the exact solution (using Bessel functions) in [11] and by the method of moments.

| Mode | k_ϕ/k [11] | Our method (k_ζ/k) | Relative error (%) |
|-------------------|-----------------|----------------------------|--------------------|
| TE _{0,1} | 0,75607 | 0,75608 | 0,00063301 |
| TE _{1,1} | $-j$ 1,1262 | $-j$ 1,1262 | 0,0031066 |
| TE _{2,1} | $-j$ 2,5856 | $-j$ 2,5857 | 0,0029801 |
| TE _{3,1} | $-j$ 3,9633 | $-j$ 3,9634 | 0,0039009 |
| TE _{4,1} | $-j$ 5,3229 | $-j$ 5,3232 | 0,0051642 |
| TE _{5,1} | $-j$ 6,6757 | $-j$ 6,6763 | 0,0084491 |
| TE _{6,1} | $-j$ 8,0252 | $-j$ 8,0264 | 0,014290 |
| TE _{7,1} | $-j$ 9,3728 | $-j$ 9,3755 | 0,029297 |
| TE _{8,1} | $-j$ 10,719 | $-j$ 10,726 | 1,062939 |
| TE _{9,1} | $-j$ 12,065 | $-j$ 12,083 | 1,15138 |

3.2.5

H-Plane with $R = 0.75a$

For $R = 0.75a$, Table 3.5 indicates the values of k_ζ/k for the H-plane. The curves of $|e_y(x)|$ for the $\text{TM}_{1,0}^y$, $\text{TM}_{2,0}^y$ and $\text{TM}_{3,0}^y$ modes are in agreement

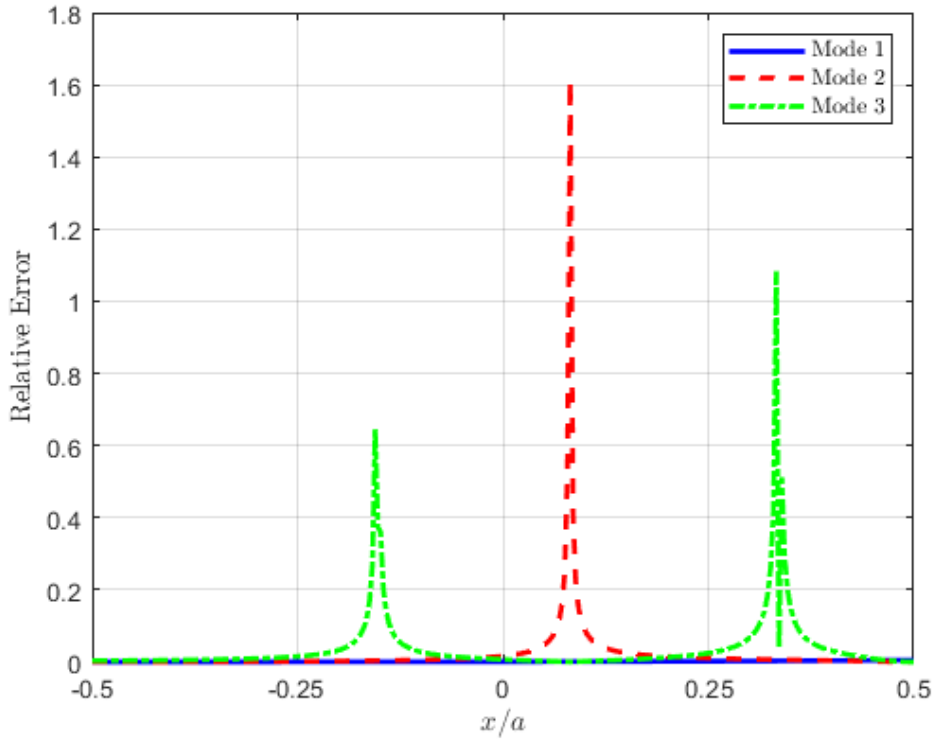


Figure 3.4: Relative error (%) of the normalized field curves $|h_y(x)|$ between PMM and MoM for $TE_{0,1}^y$, $TE_{1,1}^y$ and $TE_{2,1}^y$ modes, for $a > b$, $R = a$ and $P = 20$ points.

Table 3.5: Normalized longitudinal wavenumbers k_ϕ/k and k_ζ/k for TM modes in a rectangular waveguide curved in the H-plane (with $R = 0.75a$) obtained respectively by the exact solution (using Bessel functions) in [11] and by the method of moments.

| Mode | k_ϕ/k [11] | Our method (k_ζ/k) | Relative error (%) |
|--------------------|-----------------|----------------------------|--------------------|
| TM _{1,0} | 0,74023 | 0,74022 | 0,00084983 |
| TM _{2,0} | $-j$ 0,67168 | $-j$ 0,6767185 | 0,024851 |
| TM _{3,0} | $-j$ 1,3716 | $-j$ 1,3719 | 0,024728 |
| TM _{4,0} | $-j$ 1,9816 | $-j$ 1,9823 | 0,039431 |
| TM _{5,0} | $-j$ 2,5635 | $-j$ 2,5654 | 0,071884 |
| TM _{6,0} | $-j$ 3,1323 | $-j$ 3,1370 | 0,15176 |
| TM _{7,0} | $-j$ 3,6937 | $-j$ 3,7058 | 0,32857 |
| TM _{8,0} | $-j$ 4,2505 | $-j$ 4,2808 | 0,71104 |
| TM _{9,0} | $-j$ 4,8043 | $-j$ 4,8724 | 1,4171 |
| TM _{10,0} | $-j$ 5,3560 | $-j$ 5,4945 | 2,5851 |

with the curves in Fig. 2.6.

In Fig. 3.5, we notice that the relative error for the second mode in $0 < x/a < 0,25$ was higher than in previous scenarios. Once again, the errors for the second and third modes occur when the fields are nearly zero, and the

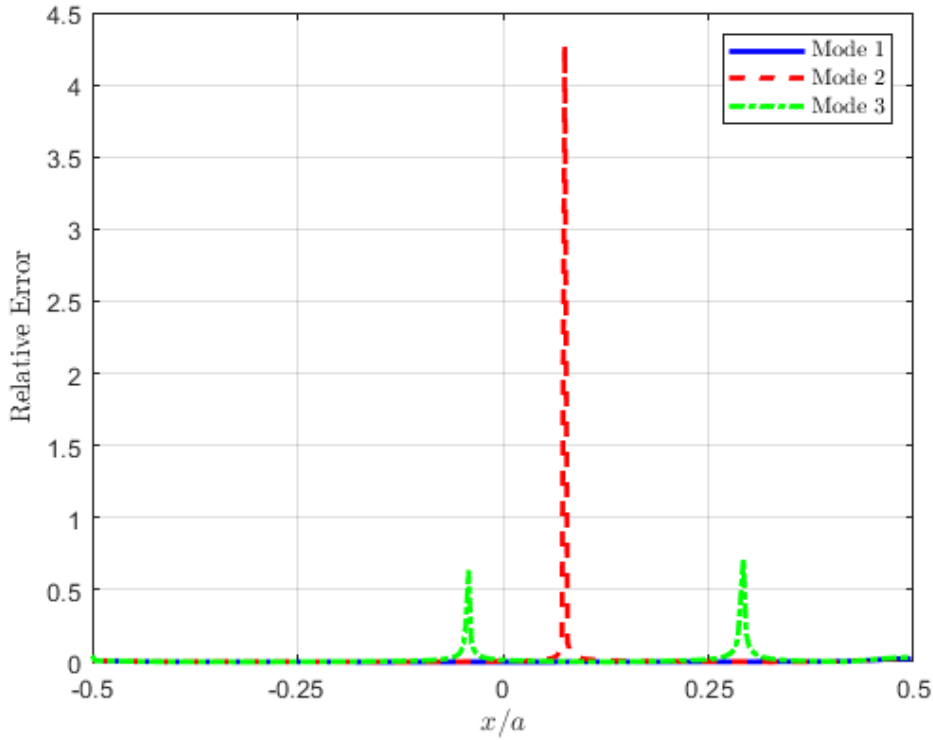


Figure 3.5: Relative error (%) of the normalized field curves $|e_y(x)|$ between PMM and MoM for $\text{TM}_{1,0}^y$, $\text{TM}_{2,0}^y$ and $\text{TM}_{3,0}^y$ modes, for $a > b$, $R = 0.75a$ and $P = 20$ points.

PMM and MoM methods are also in good agreement, especially for the $\text{TM}_{1,0}^y$ and $\text{TM}_{3,0}^y$ modes.

3.2.6

E-Plane with $R = 0.75a$

For the E-plane and $R = 0.75a$, the first ten normalized longitudinal wavenumbers for the $\text{TE}_{m,1}$ modes resulting from the method of moments are shown in Table 3.6. Similar to the H-plane, for this value of R , the relative error of the eigenvalue compared to the exact solution is less than 3%. The curves of $|h_y(x)|$ for the $\text{TE}_{0,1}^y$, $\text{TE}_{1,1}^y$, and $\text{TE}_{2,1}^y$ modes are the same as in Fig. 2.7.

In Fig. 3.6, for the E-plane, we observe that the relative errors for the $\text{TE}_{1,1}^y$ and $\text{TE}_{2,1}^y$ modes were slightly higher compared to the H-plane. For the fundamental mode, $\text{TE}_{0,1}^y$, the relative errors are practically zero.

Table 3.6: Normalized longitudinal wavenumbers k_ϕ/k and k_ζ/k for TE modes in a rectangular waveguide curved in the E-plane (with $R = 0.75a$) obtained respectively by the exact solution (using Bessel functions) in [11] and by the method of moments.

| Mode | k_ϕ/k [11] | Our method (k_ζ/k) | Relative error (%) |
|-------------------|-----------------|----------------------------|--------------------|
| TE _{0,1} | 0,75707 | 0,75710 | 0,0028950 |
| TE _{1,1} | $-j$ 0,99887 | $-j$ 0,99906 | 0,019235 |
| TE _{2,1} | $-j$ 2,3425 | $-j$ 2,3430 | 0,020766 |
| TE _{3,1} | $-j$ 3,6006 | $-j$ 3,6017 | 0,031463 |
| TE _{4,1} | $-j$ 4,8399 | $-j$ 4,8425 | 0,053895 |
| TE _{5,1} | $-j$ 6,0722 | $-j$ 6,0788 | 0,10897 |
| TE _{6,1} | $-j$ 7,3011 | $-j$ 7,3180 | 0,23216 |
| TE _{7,1} | $-j$ 8,5280 | $-j$ 8,5718 | 0,51313 |
| TE _{8,1} | $-j$ 9,7538 | $-j$ 9,8579 | 1,0677 |
| TE _{9,1} | $-j$ 10,979 | $-j$ 11,204 | 2,0555 |

Table 3.7: Normalized longitudinal wavenumbers k_ϕ/k and k_ζ/k for TM modes in a rectangular waveguide curved in the H-plane (with $R = 10a$) obtained respectively by the exact solution (using Bessel functions) in [11] and by the method of moments.

| Mode | k_ϕ/k [11] | Our method (k_ζ/k) | Relative error (%) |
|--------------------|-----------------|----------------------------|--------------------|
| TM _{1,0} | 0,75493 | 0,75493 | 0,0000033179 |
| TM _{2,0} | $-j$ 0,84756 | $-j$ 0,84756 | 0,000012749 |
| TM _{3,0} | $-j$ 1,6924 | $-j$ 1,6924 | 0,0000065975 |
| TM _{4,0} | $-j$ 2,4226 | $-j$ 2,4226 | 0,0000073101 |
| TM _{5,0} | $-j$ 3,1196 | $-j$ 3,1196 | 0,0000065350 |
| TM _{6,0} | $-j$ 3,8018 | $-j$ 3,8018 | 0,0000087165 |
| TM _{7,0} | $-j$ 4,4759 | $-j$ 4,4759 | 0,0000083743 |
| TM _{8,0} | $-j$ 5,1451 | $-j$ 5,1451 | 0,000012507 |
| TM _{9,0} | $-j$ 5,8112 | $-j$ 5,8112 | 0,000012499 |
| TM _{10,0} | $-j$ 6,4750 | $-j$ 6,4750 | 0,000021217 |

3.2.7

H-Plane with $R = 10a$

The first ten normalized longitudinal wavenumbers for the TM_{*m*,0} modes resulting from the method of moments are shown in Table 3.7. The curves of $|e_y(x)|$ for the TM_{1,0}^y, TM_{2,0}^y and TM_{3,0}^y modes are the same as in Fig. 2.8.

For this case, where $R = 10a$, the relative errors of the normalized field curves for the TM^y modes showed significantly lower values compared to other curvature radius values of the guide. For the TM_{1,0}^y mode, the result was the same as in previous cases, as expected. For the TM_{2,0}^y mode, the error was below 0,1. Finally, for the last mode, the errors were less than 0,05. This demonstrates the strong agreement and consistency between the two methods

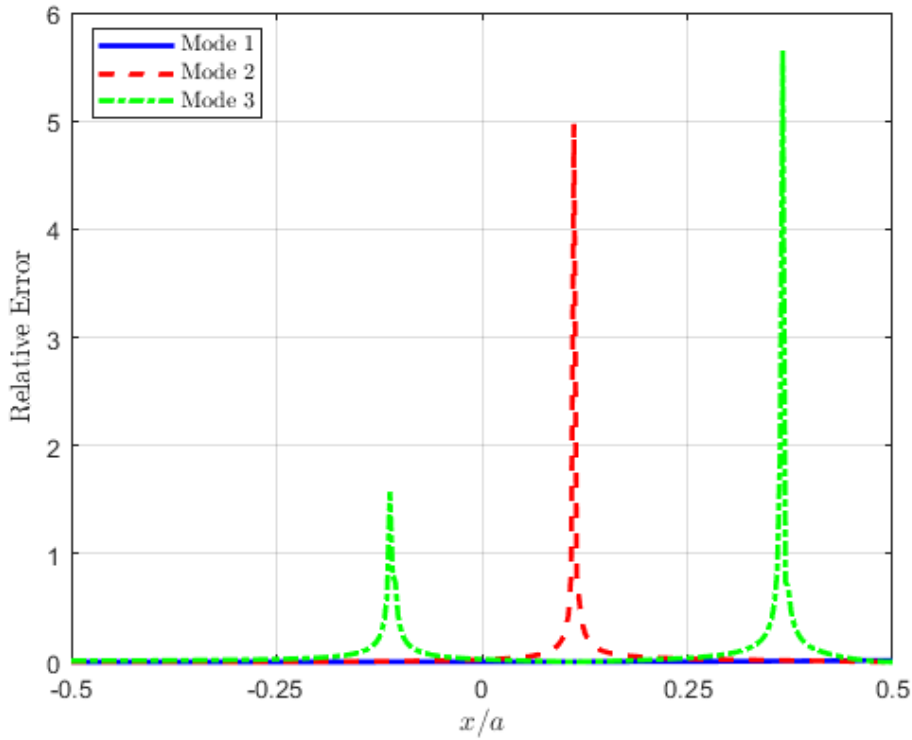


Figure 3.6: Relative error (%) of the normalized field curves $|h_y(x)|$ between PMM and MoM for $\text{TE}_{0,1}^y$, $\text{TE}_{1,1}^y$ and $\text{TE}_{2,1}^y$ modes, for $a > b$, $R = 0.75a$ and $P = 20$ points.

proposed in this thesis.

3.2.8

E-Plane with $R = 10a$

The first ten normalized longitudinal wavenumbers for the $\text{TE}_{m,1}$ modes resulting from the method of moments are shown in Table 3.8. Similar to the H-plane, for this value of R , the relative error of the eigenvalue compared to the exact solution is less than 0,00005%. The curves of $|h_y(x)|$ for the $\text{TE}_{0,1}^y$, $\text{TE}_{1,1}^y$, and $\text{TE}_{2,1}^y$ modes are the same as in Fig. 2.9.

For the E-plane, the relative errors of the $\text{TE}_{1,1}^y$ and $\text{TE}_{2,1}^y$ modes are also low, thus demonstrating good agreement between the methods. Furthermore, as in the previous scenarios, it was expected that the errors would appear when the fields are nearly zero.

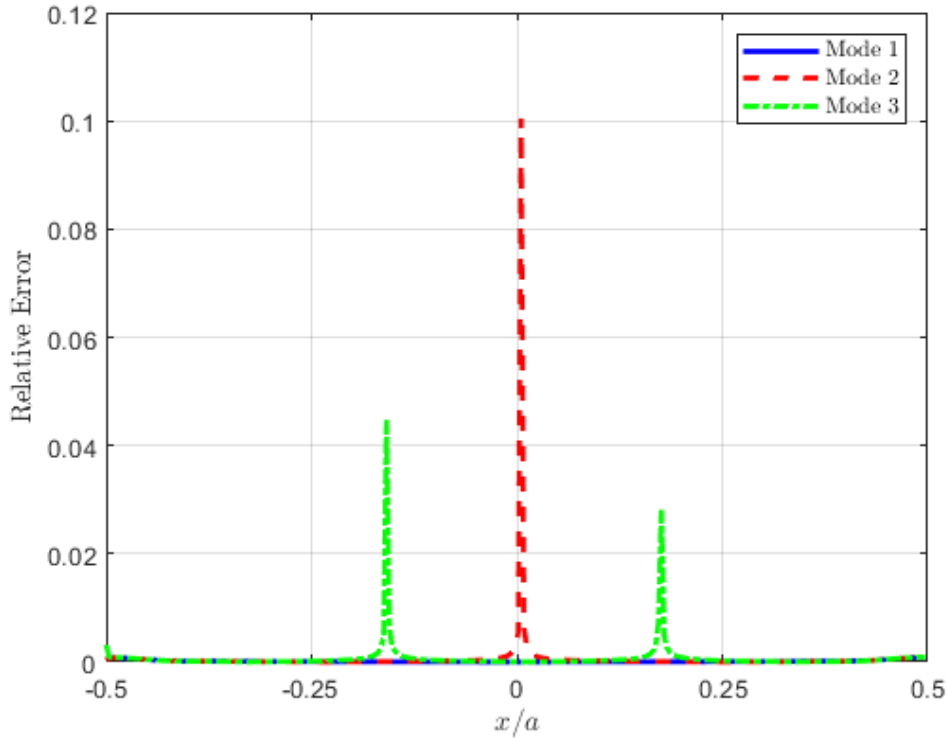


Figure 3.7: Relative error (%) of the normalized field curves $|e_y(x)|$ between PMM and MoM for $\text{TM}_{1,0}^y$, $\text{TM}_{2,0}^y$ and $\text{TM}_{3,0}^y$ modes, for $a > b$, $R = 10a$ and $P = 20$ points.

Table 3.8: Normalized longitudinal wavenumbers k_ϕ/k and k_ζ/k for TE modes in a rectangular waveguide curved in the E-plane (with $R = 10a$) obtained respectively by the exact solution (using Bessel functions) in [11] and by the method of moments.

| Mode | k_ϕ/k [11] | Our method (k_ζ/k) | Relative error (%) |
|-------------------|-----------------|----------------------------|--------------------|
| $\text{TE}_{0,1}$ | 0,75502 | 0,75502 | 0,0000017277 |
| $\text{TE}_{1,1}$ | $-j$ 1,2662 | $-j$ 1,2662 | 0,0000068546 |
| $\text{TE}_{2,1}$ | $-j$ 2,8500 | $-j$ 2,8500 | 0,0000055931 |
| $\text{TE}_{3,1}$ | $-j$ 4,3575 | $-j$ 4,3575 | 0,0000069302 |
| $\text{TE}_{4,1}$ | $-j$ 5,8480 | $-j$ 5,8480 | 0,0000064212 |
| $\text{TE}_{5,1}$ | $-j$ 7,3319 | $-j$ 7,3319 | 0,0000086823 |
| $\text{TE}_{6,1}$ | $-j$ 8,8125 | $-j$ 8,8125 | 0,0000083674 |
| $\text{TE}_{7,1}$ | $-j$ 10,291 | $-j$ 10,291 | 0,000012461 |
| $\text{TE}_{8,1}$ | $-j$ 11,769 | $-j$ 11,769 | 0,000012415 |
| $\text{TE}_{9,1}$ | $-j$ 13,246 | $-j$ 13,246 | 0,000020926 |

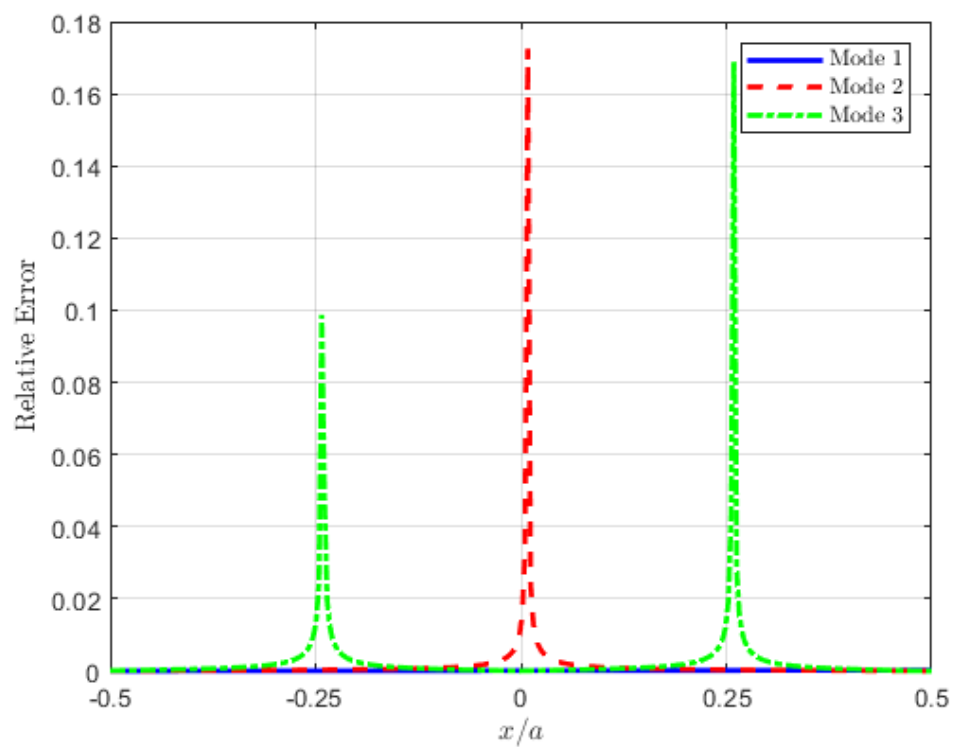


Figure 3.8: Relative error (%) of the normalized field curves $|h_y(x)|$ between PMM and MoM for $\text{TE}_{0,1}^y$, $\text{TE}_{1,1}^y$ and $\text{TE}_{2,1}^y$ modes, for $a > b$, $R = 10a$ and $P = 20$ points.

4

Comparison between the two methods presented

In this chapter, we compare the relative errors between the PMM and MoM methods to observe the performance of these techniques against the exact solution presented in [11]. Additionally, to analyze the simulation time between the two methods, we present two tables in Section 4.2 that show this comparison.

4.1

Relative Error

According to Tables 4.1– 4.8, we verify that the method of moments presented smaller relative errors compared to the exact solution [11] in relation to the point matching method. For the MoM, the relative errors were less than 2,6%, while for the PMM, the errors were below 5,1%.

Table 4.1: Relative errors of the PMM and MoM for the E-plane and $R = 0.75a$

| Mode | Relative error (%) of the PMM | Relative error (%) of the MoM |
|-------------------|-------------------------------|-------------------------------|
| TE _{0,1} | 0,22753 | 0,0028950 |
| TE _{1,1} | 1,2424 | 0,019235 |
| TE _{2,1} | 1,2146 | 0,020766 |
| TE _{3,1} | 1,2786 | 0,031463 |
| TE _{4,1} | 1,6587 | 0,053895 |
| TE _{5,1} | 1,8394 | 0,10897 |
| TE _{6,1} | 2,7714 | 0,23216 |
| TE _{7,1} | 2,8873 | 0,51313 |
| TE _{8,1} | 5,0820 | 1,0677 |
| TE _{9,1} | 4,4578 | 2,0555 |

4.2

Simulation Time

PMM simulation times are much shorter compared to MoM times, as shown in Tables 4.9 and 4.10. MoM uses an integral approach over surface functions, thus solving a dense system of linear equations. This results in a longer computational time and higher memory requirements. On the other

Table 4.2: Relative errors of the PMM and MoM for the E-plane and $R = a$

| Mode | Relative error (%) of the PMM | Relative error (%) of the MoM |
|-------------------|-------------------------------|-------------------------------|
| TE _{0,1} | 0,10267 | 0,00063301 |
| TE _{1,1} | 0,42648 | 0,0031066 |
| TE _{2,1} | 0,40852 | 0,0029801 |
| TE _{3,1} | 0,42396 | 0,0039009 |
| TE _{4,1} | 0,50453 | 0,0051642 |
| TE _{5,1} | 0,56193 | 0,0084491 |
| TE _{6,1} | 0,75467 | 0,014290 |
| TE _{7,1} | 0,85590 | 0,029297 |
| TE _{8,1} | 1,3359 | 0,062939 |
| TE _{9,1} | 1,4169 | 0,15138 |

Table 4.3: Relative errors of the PMM and MoM for the E-plane and $R = 2a$

| Mode | Relative error (%) of the PMM | Relative error (%) of the MoM |
|-------------------|-------------------------------|-------------------------------|
| TE _{0,1} | 0,021483 | 0,000061226 |
| TE _{1,1} | 0,072729 | 0,00025089 |
| TE _{2,1} | 0,069034 | 0,00021538 |
| TE _{3,1} | 0,070585 | 0,00026579 |
| TE _{4,1} | 0,078709 | 0,00027317 |
| TE _{5,1} | 0,085480 | 0,00037843 |
| TE _{6,1} | 0,10225 | 0,00043367 |
| TE _{7,1} | 0,11575 | 0,00068292 |
| TE _{8,1} | 0,15059 | 0,00090683 |
| TE _{9,1} | 0,17574 | 0,0016904 |

Table 4.4: Relative errors of the PMM and MoM for the E-plane and $R = 10a$

| Mode | Relative error (%) of the PMM | Relative error (%) of the MoM |
|-------------------|-------------------------------|-------------------------------|
| TE _{0,1} | 0,00081668 | 0,0000017277 |
| TE _{1,1} | 0,0026113 | 0,0000068546 |
| TE _{2,1} | 0,0024758 | 0,0000055931 |
| TE _{3,1} | 0,0025212 | 0,0000069302 |
| TE _{4,1} | 0,0027670 | 0,0000064212 |
| TE _{5,1} | 0,0029775 | 0,0000086823 |
| TE _{6,1} | 0,0034578 | 0,0000083674 |
| TE _{7,1} | 0,0038693 | 0,000012461 |
| TE _{8,1} | 0,0047711 | 0,000012415 |
| TE _{9,1} | 0,0055322 | 0,000020926 |

hand, PMM avoids the need for integration, simplifying the formation of the system matrix and reducing computation time.

Table 4.5: Relative errors of the PMM and MoM for the H-plane and $R = 0.75a$

| Mode | Relative error (%) of the PMM | Relative error (%) of the MoM |
|-------------------|-------------------------------|-------------------------------|
| TE _{0,1} | 0,012558 | 0,00084983 |
| TE _{1,1} | 0,28627 | 0,024851 |
| TE _{2,1} | 0,25043 | 0,024728 |
| TE _{3,1} | 0,29150 | 0,039431 |
| TE _{4,1} | 0,37747 | 0,071884 |
| TE _{5,1} | 0,52912 | 0,15176 |
| TE _{6,1} | 0,79451 | 0,32857 |
| TE _{7,1} | 1,2498 | 0,71104 |
| TE _{8,1} | 2,0005 | 1,4171 |
| TE _{9,1} | 3,1445 | 2,5851 |

Table 4.6: Relative errors of the PMM and MoM for the H-plane and $R = a$

| Mode | Relative error (%) of the PMM | Relative error (%) of the MoM |
|-------------------|-------------------------------|-------------------------------|
| TE _{0,1} | 0,0060834 | 0,00041013 |
| TE _{1,1} | 0,10114 | 0,0044792 |
| TE _{2,1} | 0,080599 | 0,0033919 |
| TE _{3,1} | 0,086194 | 0,0044001 |
| TE _{4,1} | 0,10039 | 0,0060072 |
| TE _{5,1} | 0,12392 | 0,010240 |
| TE _{6,1} | 0,16174 | 0,018223 |
| TE _{7,1} | 0,22368 | 0,038765 |
| TE _{8,1} | 0,33048 | 0,085774 |
| TE _{9,1} | 0,52018 | 0,20585 |

Table 4.7: Relative errors of the PMM and MoM for the H-plane and $R = 2a$

| Mode | Relative error (%) of the PMM | Relative error (%) of the MoM |
|-------------------|-------------------------------|-------------------------------|
| TE _{0,1} | 0,0013372 | 0,000087244 |
| TE _{1,1} | 0,017906 | 0,00042928 |
| TE _{2,1} | 0,013433 | 0,00024803 |
| TE _{3,1} | 0,013651 | 0,00028264 |
| TE _{4,1} | 0,014905 | 0,00028550 |
| TE _{5,1} | 0,016947 | 0,00039606 |
| TE _{6,1} | 0,019919 | 0,00046152 |
| TE _{7,1} | 0,024146 | 0,00073781 |
| TE _{8,1} | 0,030275 | 0,0010089 |
| TE _{9,1} | 0,039387 | 0,0019192 |

Table 4.8: Relative errors of the PMM and MoM for the H-plane and $R = 10a$

| Mode | Relative error (%) of the PMM | Relative error (%) of the MoM |
|-------------------|-------------------------------|-------------------------------|
| TE _{0,1} | 0,000051473 | 0,0000033179 |
| TE _{1,1} | 0,00065091 | 0,000012749 |
| TE _{2,1} | 0,00048084 | 0,0000065975 |
| TE _{3,1} | 0,00048265 | 0,0000073101 |
| TE _{4,1} | 0,00051900 | 0,0000065350 |
| TE _{5,1} | 0,00057881 | 0,0000087165 |
| TE _{6,1} | 0,00066396 | 0,0000083743 |
| TE _{7,1} | 0,00078058 | 0,000012507 |
| TE _{8,1} | 0,00094084 | 0,000012499 |
| TE _{9,1} | 0,0011629 | 0,000021217 |

Table 4.9: Comparison of simulation times between the PMM and MoM methods in the E-plane

| Radius of Curvature | Simulation time (s) of PMM | Simulation time (s) of MoM |
|---------------------|----------------------------|----------------------------|
| $R = 0,75a$ | 0,8105 | 85,6906 |
| $R = a$ | 0,8299 | 79,4363 |
| $R = 2a$ | 0,7639 | 148,4616 |
| $R = 10a$ | 0,8536 | 152,9791 |

Table 4.10: Comparison of simulation times between the PMM and MoM methods in the H-plane

| Radius of Curvature | Simulation time (s) of PMM | Simulation time (s) of MoM |
|---------------------|----------------------------|----------------------------|
| $R = 0,75a$ | 1,5203 | 82,2622 |
| $R = a$ | 0,8201 | 154,1584 |
| $R = 2a$ | 0,8490 | 87,7802 |
| $R = 10a$ | 0,8609 | 131,5030 |

5 Conclusions

In this thesis, we present a new PMM solution to solve the electromagnetic fields in curved rectangular waveguides. For the analyzed large and small curvature scenarios, we observed that with a reduced set of 20 harmonics, we were able to find solutions for the fundamental mode propagation constant with an error of less than 1% compared to the exact solution. The computational cost of our approach is lower than the exact approaches [11] and Galerkin's approach in [28]. Additionally, our method is relatively simple to implement numerically compared to these approaches.

Furthermore, we applied the Method of Moments to solve the fields in these guides. Similar to the PMM, for the scenarios of large and small curvature examined, it was also possible to find solutions for the propagation constant of the fundamental mode with an error of less than 1% compared to the exact solution.

With the approach of the two methods used in this work, it becomes clear that the main difference between the methods lies in the nature of the matrices involved in solving the problem and how this affects the computational time. For the point matching method, we have a matrix that is a function of the eigenvalue k_z , meaning it is not a constant matrix, and therefore, the problem is nonlinear. Despite being a nonlinear problem, the formation of this matrix is generally fast, as it only involves evaluating mathematical expressions at discrete points, without requiring numerical integration. In each iteration, the computational complexity is relatively low. Thus, the PMM requires less simulation time.

On the other hand, for the method of moments, we have constant matrices that do not depend on the eigenvalue and allow a linear eigenvalue problem. However, the construction of this constant matrix is much more complex than in PMM, as it involves integral calculations to determine the matrix coefficients. These calculations are computationally intensive and require more time and memory to perform. However, it is worth noting that despite presenting longer simulation times, the relative errors are smaller when compared to the relative errors obtained for PMM.

It is important to mention that the normalized field curves in curved

rectangular guides for the PMM and MoM methods are very similar, making it impossible to observe differences. By plotting the relative error graphs of these curves between the two methods, we found that the errors for the fundamental mode are practically negligible, and for the other two modes, the errors are very low. Thus, we can conclude that the Point Matching Method and the Method of Moments show good agreement.

Finally, as future work, we intend to investigate the convergence of PMM and MoM for dissipative problems, considering dielectric and conductive losses in the walls of the curved waveguide. Additionally, we may analyze the modeling of electromagnetic propagation in curved waveguides with other geometries, such as curved waveguides with circular, elliptical sections, among others.

Bibliography

- [1] G. Addamo, O. A. Peverini, D. Manfredi, F. Calignano, F. Paonessa, G. Virone, R. Tascone, and G. Dassano, "Additive manufacturing of ka-band dual-polarization waveguide components," *IEEE Transactions on Microwave Theory and Techniques*, vol. 66, no. 8, pp. 3589–3596, 2018.
- [2] R. F. Harrington, *Time-Harmonic Electromagnetic Fields*. New York, NY, USA: McGraw-Hill, 1961.
- [3] J. A. Cochran and R. G. Pecina, "Mode propagation in continuously curved waveguides," *Radio science*, vol. 1, no. 6, pp. 679–696, 1966.
- [4] L. Lewin, D. Chang, and E. Kuester, *Electromagnetic waves and curved structures*. London, UK: Peter Peregrinus, 1977.
- [5] K. W. Kark, "Perturbation analysis of electromagnetic eigenmodes in toroidal waveguides," *IEEE transactions on microwave theory and techniques*, vol. 39, no. 4, pp. 631–637, 1991.
- [6] A. Weisshaar, S. M. Goodnick, and V. K. Tripathi, "A rigorous and efficient method of moments solution for curved waveguide bends," *IEEE Transactions on microwave theory and techniques*, vol. 40, no. 12, pp. 2200–2206, 1992.
- [7] G. S. Rosa, "A mode-matching-based formulation for the analysis of curved rectangular waveguides," *IEEE Transactions on Microwave Theory and Techniques*, 2023.
- [8] B. Gimeno and M. Guglielmi, "Multimode equivalent network representation for h-and e-plane uniform bends in rectangular waveguide," *IEEE Transactions on microwave theory and techniques*, vol. 44, no. 10, pp. 1679–1687, 1996.
- [9] P. Cornet, R. Dusseaux, and J. Chandezon, "Wave propagation in curved waveguides of rectangular cross section," *IEEE Transactions on microwave theory and techniques*, vol. 47, no. 7, pp. 965–972, 1999.
- [10] A. Blas, B. Gimeno, V. Boria, H. Esteban, S. Cogollos, and A. Coves, "A rigorous and efficient full-wave analysis of uniform bends in rectangular waveguide under arbitrary incidence," *IEEE Transactions on microwave theory and techniques*, vol. 51, no. 2, pp. 397–405, 2003.

- [11] G. S. Rosa, "An accurate and numerically stable formulation for computing the electromagnetic fields in uniform bend rectangular waveguides," *IEEE Transactions on Microwave Theory and Techniques*, vol. 71, no. 3, pp. 988–996, 2022.
- [12] R. Bates, "The point-matching method for interior and exterior two-dimensional boundary value problems (correspondence)," *IEEE Transactions on Microwave Theory and Techniques*, vol. 15, no. 3, pp. 185–187, 1967.
- [13] J. R. Gonçalves, "Semi-analytical methods for the electromagnetic propagation analysis of inhomogeneous anisotropic waveguides of arbitrary cross-section by using cylindrical harmonics," Ph.D. dissertation, PUC-Rio, 2022.
- [14] R. Bates and F. Ng, "Point matching computation of transverse resonances," *International Journal for Numerical Methods in Engineering*, vol. 6, no. 2, pp. 155–168, 1973.
- [15] H. Yee and N. Audeh, "Uniform waveguides with arbitrary cross-section considered by the point-matching method," *IEEE Transactions on Microwave Theory and Techniques*, vol. 13, no. 6, pp. 847–851, 1965.
- [16] S. Ranade and A. Rosenfeld, "Point pattern matching by relaxation," *Pattern recognition*, vol. 12, no. 4, pp. 269–275, 1980.
- [17] S. Shu, P. Goggans, and A. Kishk, "Computation of cutoff wavenumbers for partially filled waveguide of arbitrary cross section using surface integral formulations and the method of moments," *IEEE transactions on microwave theory and techniques*, vol. 41, no. 6, pp. 1111–1118, 1993.
- [18] P. R. de Jesus Dantas, "Mathematical modeling of curved rectangular waveguides using the variational rayleigh-ritz method," Ph.D. dissertation, PUC-Rio, 2023.
- [19] P. Moon and D. E. Spencer, "The meaning of the vector laplacian," *Journal of the Franklin Institute*, vol. 256, no. 6, pp. 551–558, 1953.
- [20] J. A. Stratton, *Electromagnetic theory*. John Wiley & Sons, 2007, vol. 33.
- [21] P. Moon and D. E. Spencer, "Separability conditions for the laplace and helmholtz equations," *Journal of the Franklin Institute*, vol. 253, no. 6, pp. 585–600, 1952.
- [22] D. E. Spencer, "Separation of variables in electromagnetic theory," *Journal of Applied Physics*, vol. 22, no. 4, pp. 386–389, 1951.

- [23] G. S. Rosa, "Pseudo-analytical modeling for electromagnetic well-logging tools in complex geophysical formations," Ph.D. dissertation, Dept. Elect. Eng., Pontifical Catholic University of Rio de Janeiro, Rio de Janeiro, RJ, Brazil, 2017.
- [24] G. S. Rosa, J. R. Bergmann, and F. L. Teixeira, "A perturbation method to model electromagnetic well-logging tools in curved boreholes," *IEEE Trans. Geosci. Remote Sens.*, vol. 56, no. 4, pp. 1979–1993, Apr. 2018, DOI: 10.1109/TGRS.2017.2771723.
- [25] —, "Axial mode-matching technique for analysis of directional well-logging sensor tools," in *IEEE International Symposium on Antennas and Propagation/USNC-URSI National Radio Science*, Fajardo, Puerto Rico, Jun. 26–Jul. 1st 2016, pp. 2041–2042, DOI: 10.1109/APS.2016.7696727.
- [26] I. The MathWorks, *MATLAB R2024a*, The MathWorks, Inc., Natick, Massachusetts, United States, 2024, available at <https://www.mathworks.com/products/matlab.html>.
- [27] W. C. Gibson, *The method of moments in electromagnetics*. Chapman and Hall/CRC, 2021.
- [28] R. Harrington, *Field computation by moment methods*. Piscataway, NJ: IEEE Press, 1993.
- [29] C. A. Balanis, *Advanced engineering electromagnetics*. John Wiley & Sons, 2012.